JEM Journal of Experimental Medicine

ARTICLE

STAT3 regulates CD8⁺ T cell differentiation and functions in cancer and acute infection

Qinli Sun[1], Xiaohong Zhao[1], Ruifeng Li[1,2], Dingfeng Liu[3,4], Birui Pan[1], Bowen Xie[1,2], Xinxin Chi[1], Dongli Cai[3,4], Peng Wei[1,2], Wei Xu[1,2], Kun Wei[1], Zixuan Zhao[1], Yujie Fu[1,4], Ling Ni[1], and Chen Dong[1,2,4,5]

In cancer, persistent antigens drive CD8⁺ T cell differentiation into exhausted progenitor (T_{ex}^{prog}) and terminally exhausted (T_{ex}^{term}) cells. However, how the extrinsic and intrinsic regulatory mechanisms cooperate during this process still remains not well understood. Here, we found that STAT3 signaling plays essential roles in promoting intratumor T_{ex}^{term} cell development by enhancing their effector functions and survival, which results in better tumor control. In tumor microenvironments, STAT3 is predominantly activated by IL-10 and IL-21, but not IL-6. Besides, STAT3 also plays critical roles in the development and function of terminally differentiated effector CD8⁺ T cells in acute infection. Mechanistically, STAT3 transcriptionally promotes the expression of effector function-related genes, while it suppresses those expressed by the progenitor T_{ex} subset. Moreover, STAT3 functions in collaboration with BATF and IRF4 to mediate chromatin activation at the effector gene loci. Thus, we have elucidated the roles of STAT3 signaling in terminally differentiated CD8⁺ T cell development, especially in cancer, which benefits the development of more effective immunotherapies against tumors.

Introduction

In acute infection and vaccination, effector CD8⁺ T cells develop into two subpopulations: one subpopulation is KLRG1⁺IL-7R^{low} short-lived effector CD8⁺ T cells, also termed terminally differentiated effector CD8⁺ T cells, and another, KLRG1⁻IL-7R^{hi} memory precursors, which can subsequently develop into memory CD8⁺ T cells after the clearance of antigens (Joshi et al., 2007; Rutishauser et al., 2009). However, in cancer and chronic infection, persistent antigenic stimulation drives CD8⁺ T cells into an exhaustion state (McLane et al., 2019; Pauken and Wherry, 2015). Exhausted CD8⁺ T cells (T_{ex}) are functionally distinct from effector and memory CD8⁺ T cells observed in acute infections and are characterized by elevated expression of inhibitory receptors (PD-1, LAG3, TIGIT, etc.), poor effector functions, altered epigenetic and transcriptional landscapes, and skewed metabolic status (McLane et al., 2019). Similar to the classification of effector CD8⁺ T cells, in cancer, tumor-specific T_{ex} cells are mainly classified into two subpopulations, named progenitors (T_{ex}^{prog}) and terminally differentiated CD8⁺ T (T_{ex}^{term}) cells (Miller et al., 2019; Siddiqui et al., 2019). Tumor-specific T_{ex}^{prog} cells are stem-like and highly express TCF1 transcription factor, which persist long term and are capable of differentiating into T_{ex}^{term} cells for long-term tumor control (Miller et al., 2019; Siddiqui et al., 2019). A distinguishing feature of memory CD8⁺ T cells is their ability to rapidly expand and efficiently generate effector functions in response to antigen re-stimulation. Although T_{ex}^{prog} cells are stem-like, their memory potentials are progressively lost and not at the levels of memory CD8⁺ T cells generated in acute infection (Angelosanto et al., 2012; Huang et al., 2022; Kaech and Cui, 2012; McLane et al., 2019). In contrast, tumor-specific TIM-3⁺ T_{ex}^{term} cells have characteristics of potent cytotoxicity, active proliferative capacity, and high-level apoptosis (Miller et al., 2019; Siddiqui et al., 2019). However, the transcriptional and epigenetic mechanisms underlying CD8⁺ T cell differentiation and maintenance, especially T_{ex}^{term} cells in cancer, remain elusive, and the cell-intrinsic and -extrinsic factors controlling T_{ex} cell differentiation also need to be further identified.

T cell differentiation is generally regulated by three signals: signal 1 from antigen receptors, signal 2 from costimulatory or inhibitory molecules, and signal 3 from inflammatory cytokines (McLane et al., 2019). During chronic infection and cancer, persistent T cell receptor stimulation sustains the activation of

[1]Institute for Immunology, Tsinghua University, Beijing, China; [2]Tsinghua-Peking Center for Life Sciences, Tsinghua University, Beijing, China; [3]Department of Gynaecology, Shanghai First Maternity and Infant Hospital, School of Medicine, Tongji University, Shanghai, China; [4]Shanghai Immune Therapy Institute, Shanghai Jiao Tong University School of Medicine-Affiliated Renji Hospital, Shanghai, China; [5]Research Unit of Immune Regulation and Immune Diseases of Chinese Academy of Medical Sciences, Shanghai Jiao Tong University School of Medicine-Affiliated Renji Hospital, Shanghai, China.

Correspondence to Chen Dong: chendong@tsinghua.edu.cn.

NFAT and induces high-level expression of TOX and Nr4a1, which limit T cell function and promote T cell exhaustion (Chen et al., 2019; Khan et al., 2019; Liu et al., 2019; Martinez et al., 2015; Scott et al., 2019). In addition, elevated expression of co-inhibitory receptors (e.g., PD-1 and CTLA-4) in T_{ex} cells also enforces exhaustion, and the blockade of their signaling has shown clinical benefits in various human cancer types (Callahan et al., 2016; Kamphorst et al., 2017). Moreover, it has been reported that diminished TCR and costimulatory signaling in established chronic infection preferentially programs T_{ex} cells into TCF1$^+$ memory-like subset (Snell et al., 2018). Importantly, in addition to TCR and costimulatory/inhibitory molecules, T_{ex} cell generation is also shaped by a broad range of inflammatory cytokines (McLane et al., 2019). Among them, JAK-STAT cytokines are critical in regulating T cell development in immune responses (Dong, 2021). For example, STAT1 is critical in promoting T cell expansion and antitumor response in cancer (Ryan et al., 2020). Consistently, STAT1 upstream cytokines, including type I IFN and IL-27, function to drive TIM-3$^+$ T_{ex} cell differentiation in both cancer and chronic infection (Chihara et al., 2018; Wu et al., 2016; Yang et al., 2012). In addition, IL-2–STAT5 axis functions as an inducer of exhaustion and promotes the generation of TIM-3$^+$ T_{ex} cells within tumors (Liu et al., 2021).

STAT3 is a cytoplasmic transcription factor belonging to the signal transducer and activators of transcription (STAT) family (Darnell, 1997). It can be phosphorylated and activated by multiple cytokines (e.g., IL-6, IL-10, IL-21, and IL-23), and it transcriptionally regulates the fate decisions of various CD4$^+$ T lymphocyte lineages (Dong, 2021). The IL-6/IL-23–STAT3 axis induces RORγt expression during Th17 cell development (Chang et al., 2020; Yang et al., 2007), and the IL-6/IL-21–STAT3 pathway also promotes Bcl6 expression during Tfh cell differentiation (Nurieva et al., 2009; Xu et al., 2019). However, the role of STAT3 in regulating CD8$^+$ T cell differentiation and function remains controversial and lacks mechanistic understanding. More importantly, its role in tumor-specific T_{ex} cell development still remains unclear. STAT3 was long considered to promote memory CD8$^+$ T cell development (Cui et al., 2011; Hanna et al., 2021; Olson and Jameson, 2011; Siegel et al., 2011). A previous study showed that *Stat3* deficiency impaired the maturation and self-renewal of IL-7R^{hi}KLRG1^{low} memory CD8$^+$ T cells in acute LCMV virus–infected mice (Cui et al., 2011). The development and maintenance of human central memory CD8$^+$ T cells were also diminished in autosomal-dominant hyper-IgE syndrome patients with STAT3 mutations (Siegel et al., 2011). Moreover, in the chronic lymphocytic leukemia model, *Stat3* deletion lowered the frequencies of memory-like PD-1^{int}TCF-1$^+$ CD8$^+$ T cells (Hanna et al., 2021), and the leptin-induced STAT3 activation in obesity-driven breast cancer inhibited IFN-γ production and CD8$^+$ T cell effector function (Zhang et al., 2020). However, contrary to these findings, another study showed that *Stat3* deficiency decreased KLRG-1$^+$ effector CD8$^+$ T cells in HSV-1 infection (Yu et al., 2013) and reduced the expression of Blimp1, BATF, and Granzyme B in IL-21–stimulated CD8$^+$ T cells in vitro (Xin et al., 2015). Thus, the role of STAT3 signaling in CD8$^+$ T cell differentiation and function, especially in the context of tumor antigen–driven exhaustion, urgently needs to be clarified via a detailed mechanistic approach, and its upstream inducers within the tumors also need to be systematically identified.

In this study, we illustrated the function of STAT3 signaling in terminally differentiated CD8$^+$ T cells, especially in cancer. Activated by IL-10 and IL-21, STAT3 played critical roles in promoting tumor-specific T_{ex}^{term} cell development and their effector functions in cancer. It was also intrinsically critical in promoting the development and function of terminally differentiated effector CD8$^+$ T cells in acute infection. Mechanistically, STAT3 transcriptionally promoted the expression of T_{ex}^{term}-associated genes and inhibited that of T_{ex}^{prog} genes, thus enforcing the T_{ex}^{term} transcriptional program. STAT3 functioned by epigenetically activating multiple T_{ex}^{term}-related gene loci. In addition, STAT3 cooperated with BATF and IRF4 to mediate T_{ex}^{term} cell differentiation. Altogether, this study has mechanistically clarified the role of STAT3 signaling in terminally differentiated CD8$^+$ T cells, especially in cancer, which may benefit the development of novel cancer immunotherapies.

Results

STAT3 promotes the effector function of CD8$^+$ T cells

To first understand the function of STAT3 in the regulation of anti-cancer CD8$^+$ T cells, we analyzed public single-cell RNA sequencing (scRNA-seq) data of human patients with lung cancer, colorectal cancer (CRC), and hepatocellular carcinoma (HCC; Guo et al., 2018; Zhang et al., 2018; Zheng et al., 2017). We found that *STAT3* expression was elevated in tumor-infiltrating CD8$^+$ T cells, especially in PD-1$^+$ T_{ex} cells, as compared with peripheral CD8$^+$ T cells in the blood (Fig. S1 A). High levels of *Stat3* expression were also found in tumor-infiltrating CD8$^+$ T cells in murine B16-OVA and E.G7 tumor models at both transcriptional and protein levels (Fig. S1, B and C).

To investigate the function of STAT3 in anti-tumor CD8$^+$ T cells, we generated *Stat3*$^{fl/fl}$*Cd8a*^{Cre} mice, in which *Stat3* was specifically deleted in mature CD8$^+$ T cells (Maekawa et al., 2008; Takeda et al., 1998). CD8$^+$ T cell development was intact in the thymus and peripheral lymphoid organs in 6–8-wk-old *Stat3*$^{fl/fl}$*Cd8a*^{Cre} mice as compared with *Stat3*$^{fl/fl}$ mice (Fig. S1, D and E), and their homeostasis in peripheral spleens and lymph nodes was not significantly affected by the deficiency of *Stat3* (Fig. S1 F). To further explore the roles of STAT3 in CD8$^+$ T cell function in tumor models, we inoculated *Stat3*$^{fl/fl}$*Cd8a*^{Cre} mice, as well as *Stat3*$^{fl/fl}$ control mice, with B16-OVA or E.G7 tumor cells. We found that *Stat3* deficiency in CD8$^+$ T cells resulted in enhanced growth of B16-OVA and E.G7 tumors (Fig. 1 A). As a result of *Stat3* deficiency, the numbers of CD8$^+$ T cells decreased substantially in both tumor-draining lymph nodes (TDLNs) and tumors (Fig. 1 B), and so did the ratio of CD8$^+$ T cells to CD4$^+$ T cells (Fig. S1 G). More importantly, the frequencies of OVA-specific tumor-infiltrating CD8$^+$ T cells (TILs) and CD44$^+$PD-1$^+$ antigen–experienced CD8$^+$ TILs were significantly reduced in E.G7-bearing *Stat3*$^{fl/fl}$*Cd8a*^{Cre} mice (Fig. S1, H and I). In addition, the cytotoxic function of PD-1$^+$–exhausted *Stat3*$^{-/-}$ CD8$^+$ T cells was dramatically reduced as indicated by decreased production of IFN-γ and Granzyme B in both B16-OVA and E.G7 models

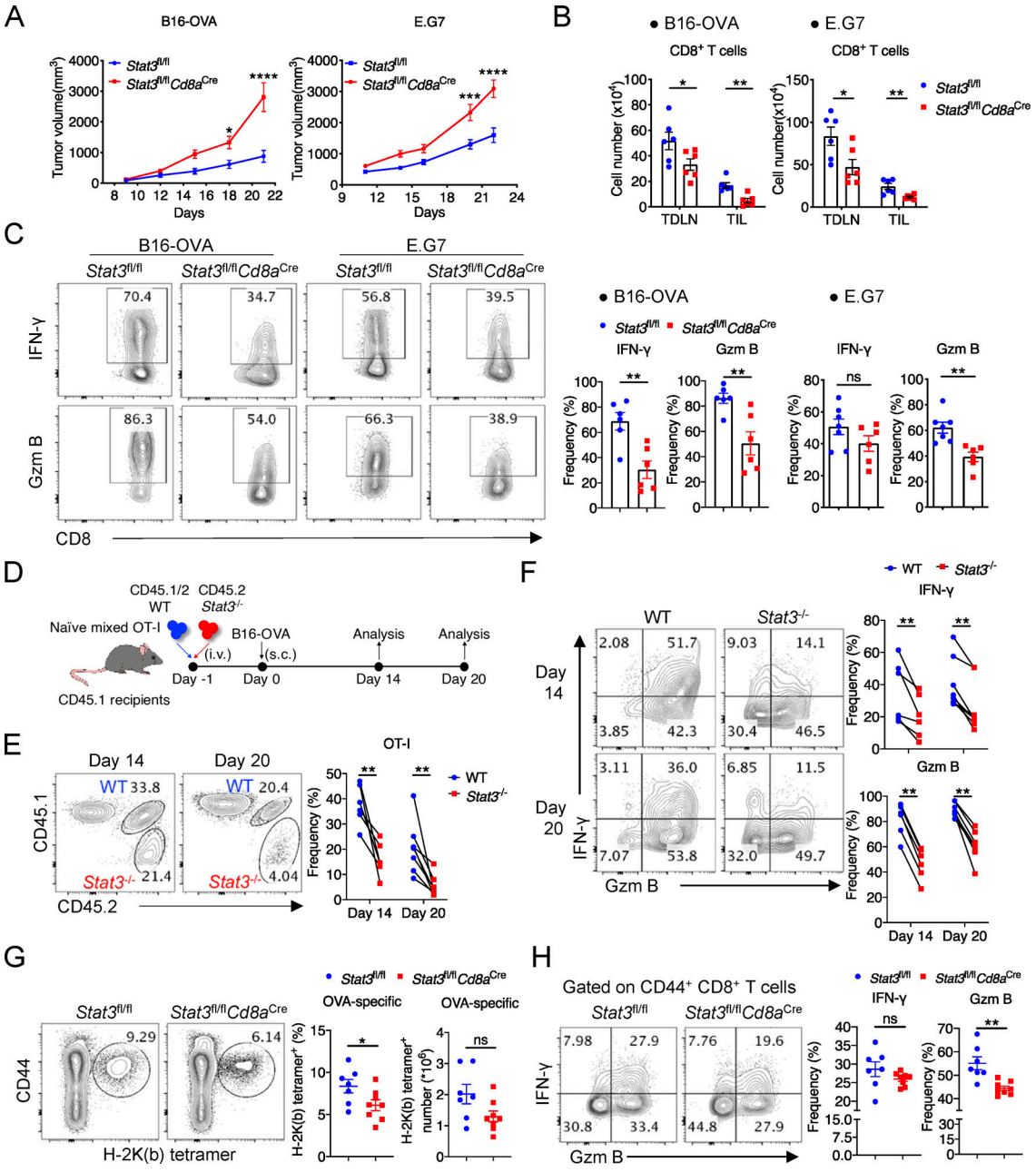

Figure 1. **STAT3 promotes the effector function of CD8⁺ T cells. (A)** Mean volumes of B16-OVA tumors (left panel) in *Stat3*$^{fl/fl}$ (n = 6) and *Stat3*$^{fl/fl}$*Cd8a*^{Cre} (n = 6) mice, or E.G7 tumors (right panel) in *Stat3*$^{fl/fl}$ (n = 7) and *Stat3*$^{fl/fl}$*Cd8a*^{Cre} (n = 6) mice. **(B)** Numbers of CD8⁺ T cells in TDLNs and tumors from *Stat3*$^{fl/fl}$ and *Stat3*$^{fl/fl}$*Cd8a*^{Cre} mice. **(C)** Representative plots (left panel) and quantifications (right panel) of IFN-γ and Granzyme B production in CD44⁺PD-1⁺ CD8⁺ TILs from B16-OVA (left panel) or E.G7 (right panel) tumors. **(D)** Experimental design for adoptive cotransfer of naive WT and *Stat3*$^{-/-}$ OT-I cells and B16-OVA tumor–challenge assay. **(E)** OT-I TIL frequencies among total CD8⁺TILs from B16-OVA tumors on day 14 and day 20 after tumor inoculation. **(F)** Representative plots (left panel) and quantifications (right panel) of IFN-γ and Granzyme B production in OT-I TILs from B16-OVA tumors. **(G)** Frequencies of OVA-specific CD8⁺ T cells and their numbers (P = 0.0590) in LM-OVA–infected *Stat3*$^{fl/fl}$ and *Stat3*$^{fl/fl}$*Cd8a*^{Cre} mice on day 8. **(H)** Representative plots (left panel) and quantifications (right panel) of IFN-γ and Granzyme B production in splenic CD44⁺ CD8⁺ T cells on day 8 after LM-OVA infection. Data are representative of two (A [left], B [left], C [left], G, and H) or three (A [right], B [right], C [right], and D–F) independent experiments. Data are shown as mean ± SEM. *, P < 0.05; **, P < 0.01; ***, P < 0.001; ****, P < 0.0001 by two-way ANOVA (A), unpaired two-tailed Student's *t* test (B, C, G, and H), or paired two-tailed Student's *t* test (E and F).

(Fig. 1 C). These data indicated a critical role of STAT3 in anti-tumor response of CD8⁺ T cells.

To further understand the function of STAT3 in tumor-specific CD8⁺ T cells and to rule out the impact of tumor volumes, we crossed *Stat3*$^{fl/fl}$*Cd8a*^{Cre} mice into CD45.2 OT-I strain and cotransferred equal numbers of their naive OT-I cells and CD45.1/2 WT OT-I cells into CD45.1 recipients with B16-OVA tumors (Fig. 1 D). Consistent with the above results, the frequencies of *Stat3*$^{-/-}$ OT-I cells among total CD8⁺ TILs were dramatically reduced as compared with WT OT-I cells on both

day 14 and day 20 after inoculation (Fig. 1 E). The percentages of *Stat3*$^{-/-}$ OT-I cells were also substantially decreased in TDLNs on day 20 (Fig. S1 J). Importantly, IFN-γ and Granzyme B production was significantly defective in *Stat3*$^{-/-}$ OT-I TILs (Fig. 1 F). However, Ki-67 expression in OT-I TILs was not affected by *Stat3* deficiency (Fig. S1 K). These results demonstrated that STAT3 was intrinsically required for the homeostasis and cytotoxic function of CD8$^+$ T cells in cancer.

We next examined STAT3 functions in effector CD8$^+$ T cells using an acute infection model. We infected *Stat3*$^{fl/fl}$*Cd8a*^{Cre} mice and their littermate *Stat3*$^{fl/fl}$ mice with *Listeria*-OVA (LM-OVA) bacteria and analyzed them on day 8. Consistent with the data in tumor models, reduced percentages and numbers of OVA-specific CD8$^+$ T cells were observed in spleens from infected *Stat3*$^{fl/fl}$*Cd8a*^{Cre} mice (Fig. 1 G), and the percentages of Granzyme B–producing cells were significantly decreased by *Stat3* deletion in splenic CD8$^+$ T cells (Fig. 1 H). However, the frequency of Ki-67–expressing cells was comparable in *Stat3*$^{fl/fl}$*Cd8a*^{Cre} and *Stat3*$^{fl/fl}$ mice (Fig. S1 L). These results altogether indicated a critical role of STAT3 in the homeostasis and function of terminally differentiated CD8$^+$ T cells in both tumor and acute infection models.

STAT3 promotes the development of terminally differentiated CD8$^+$ T cells

Since T_{ex}^{term} vs. T_{ex}^{prog} cells mediate the cytotoxic function and long-term maintenance of T_{ex} cells, respectively (Miller et al., 2019), we next investigated whether STAT3 plays any role in the regulation of tumor-specific T_{ex} cell fates. By analyzing co-transferred WT and *Stat3*$^{-/-}$ OT-I cells from B16-OVA tumors, we found that the percentages of Ly108$^-$TIM-3$^+$ T_{ex}^{term} cells were dramatically reduced, while those of Ly108$^+$TIM-3$^-$ T_{ex}^{prog} cells were significantly increased by the deficiency of *Stat3* on both day 14 and day 20 (Fig. 2 A). Importantly, both the T_{ex}^{term} and T_{ex}^{prog} TIL numbers significantly decreased as a result of the deficiency in *Stat3* on day 14 and day 20, and T_{ex}^{term} cells were reduced to a greater extent than T_{ex}^{prog} cells (Fig. 2, B and A). Moreover, by comparing the numbers of T_{ex}^{term} and T_{ex}^{prog} TILs between day 14 and day 20, we found that the maintenance of T_{ex}^{term} and T_{ex}^{prog} cells was both decreased by the deletion of *Stat3*, especially the T_{ex}^{term} cells (Fig. 2 B). Consistently, decreased frequencies of TIM-3$^+$ cells in *Stat3*$^{-/-}$ OT-I cells were also observed in TDLNs, while almost all OT-I cells were maintained as Ly108$^+$ progenitor cells and a lesser number was TIM-3$^+$ T_{ex}^{term} cells in TDLNs, as previously reported (Schenkel et al., 2021; Fig. S2 B). In addition, the frequencies of TCF1$^+$ and Bcl6$^+$Blimp1$^-$ cells in *Stat3*$^{-/-}$ OT-I TILs became higher than those in WT OT-I TILs, while the percentages of CX3CR1$^+$Ly108$^-$ and Bcl6$^-$Blimp1$^+$ cells in *Stat3*$^{-/-}$ OT-I TILs significantly decreased (Fig. S2, C and D). Moreover, the mean fluorescence intensities of TOX staining in *Stat3*$^{-/-}$ OT-I TILs increased, while those of T-bet decreased as compared with WT OT-I TILs (Fig. S2 E). These results indicated that STAT3 might function to promote T_{ex}^{term} vs. T_{ex}^{prog} cell differentiation, and it was also critical for the maintenance of T_{ex} cells, especially the T_{ex}^{term} cells.

To further analyze tumor-specific *Stat3*$^{-/-}$ CD8$^+$ TILs at the transcriptional level, we performed RNA-seq for cotransferred WT and *Stat3*$^{-/-}$ OT-I TILs from B16-OVA tumors on about day 16. Consistent with the above flow cytometry results, GSEA (Gene Set Enrichment Analysis) results revealed that the transcriptome of WT OT-I TILs was relatively more similar with TCF1$^-$ T_{ex}^{term} subset, while *Stat3*$^{-/-}$ OT-I TILs were more transcriptionally related to TCF1$^+$ T_{ex}^{prog} cells (Fig. 2 C). In addition, signature genes of effector CD8$^+$ T cells and Th1 cells were more enriched in WT OT-I TILs, while those of memory CD8$^+$ T cells and Tfh cells were relatively concentrated in *Stat3*$^{-/-}$ OT-I TILs (Fig. S2 F). The expression of 263 genes was significantly downregulated in *Stat3*$^{-/-}$ OT-I TILs, while that of 381 genes was elevated by the deficiency of *Stat3* (Fig. S2 G and Table S1). Specifically, the mRNA expression of T_{ex}^{term}-related surface molecules (*Havcr2*, *Entpd1*, *Cx3cr1*, etc.) and transcriptional factors (*Prdm1*, *Id2*, *Batf*, etc.) was significantly downregulated, while the expression of numerous T_{ex}^{prog}-associated surface molecules (*Cxcr5*, *Ccr7*, *Slamf6*, *Btla*, etc.) and transcriptional factors (*Tcf7*, *Id3*, *Bcl6*, *Bach2*, etc.) was upregulated in *Stat3*$^{-/-}$ OT-I TILs (Fig. 2 D), which were consistent with their protein expression. In addition, pathway analyses revealed that several cell killing–related pathways were downregulated in *Stat3*$^{-/-}$ OT-I TILs (Fig. 2 E), consistent with the decreased expression of cytotoxic molecules (*Gzmb* and *Ifng*) at both transcriptional and protein levels. Moreover, multiple pathways involved in lymphocyte differentiation, activation, adhesion, and migration were also significantly affected by the deficiency of *Stat3* (Fig. 2 E). However, the expression of many cell cycle–related genes was comparable in WT and *Stat3*$^{-/-}$ OT-I TILs at the transcriptional level (Fig. S2 H), which was consistent with the above Ki-67 staining results (Fig. S1 K), indicating that STAT3 might have limited effect on CD8$^+$ T cell proliferation in tumors. In addition, GSEA analysis revealed that genes involved in the OXPHOS pathway were relatively enriched in WT OT-I cells as compared with *Stat3*$^{-/-}$ OT-I TILs, and mRNA levels for some of them decreased dramatically in *Stat3*$^{-/-}$ OT-I TILs (Fig. S2, I and J). These results suggested that STAT3 might be critical in promoting OXPHOS and maintaining the mitochondrial fitness of T_{ex} cells within tumors, which was consistent with its functions previously found in regulating cellular respiration and homeostasis (Huynh et al., 2019; Wegrzyn et al., 2009).

To further analyze the specific roles of STAT3 in regulating the cytotoxic function of T_{ex}^{prog} and T_{ex}^{term} cells, we assessed the Granzyme B expression in *Stat3*$^{-/-}$ T_{ex}^{prog} and T_{ex}^{term} cells. Granzyme B expression levels were significantly reduced in *Stat3*-deficient T_{ex}^{term} cells, while those in T_{ex}^{prog} cells were not affected, as compared with the corresponding WT cells (Fig. 2 F), indicating that STAT3 might play more important roles in promoting the cytolytic function of T_{ex}^{term} cells.

To further analyze the role of STAT3 in antigen-specific CD8$^+$ T cells in acute infection, we next adoptively cotransferred naive CD45.1/2 WT and CD45.2 *Stat3*$^{-/-}$ OT-I cells at 1:1 ratio into CD45.1 recipients 1 d prior to LM-OVA infection. Consistent with the results in tumors, TCF1$^-$Granzyme B$^+$ cell frequencies were significantly reduced and TCF1$^+$Granzyme B$^-$ cell percentages were increased in the absence of *Stat3* (Fig. 2 G). T-bet expression levels were also downregulated in splenic *Stat3*$^{-/-}$ OT-I cells (Fig. S2 K). Consistently, the percentages of CD127$^-$KLRG1$^+$

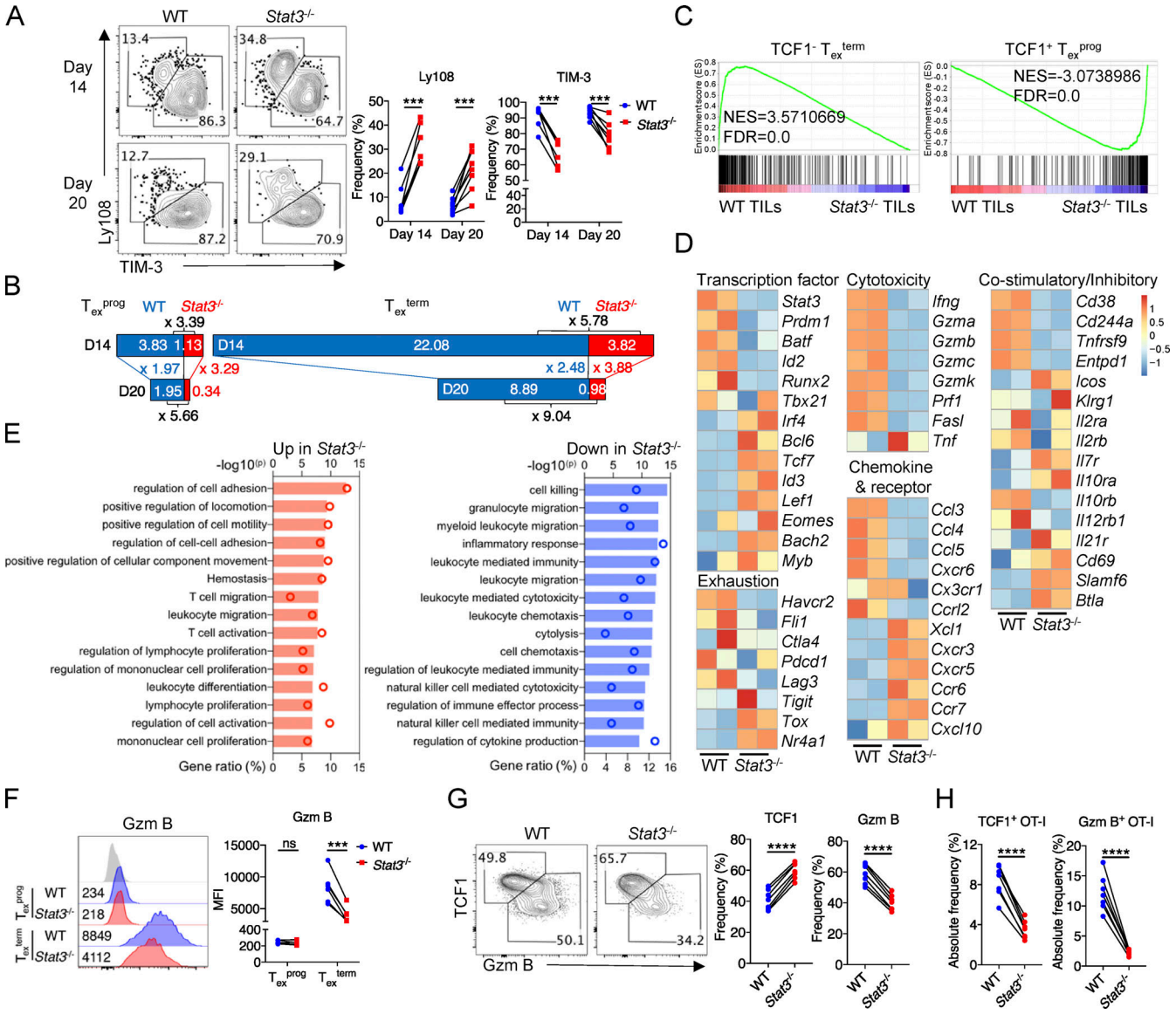

Figure 2. **STAT3 promotes the development of terminally differentiated CD8⁺ T cells. (A)** Representative plots (left panel) and quantifications (right panel) of Ly108 and TIM-3 expression on OT-I cells from B16-OVA tumors on day 14 and day 20 after tumor inoculation. **(B)** Stacked bar graphs showing the numbers (× 10^4) of Ly108⁺TIM-3⁻ T_{ex}^{prog} and Ly108⁻TIM-3⁺ T_{ex}^{term} cells based on experimental results in Fig. S2 A. The width of the stacked bar represents cell numbers (× 10^4). **(C)** GSEA results for identifying gene signatures of WT and *Stat3*$^{-/-}$ OT-I TILs compared with other T cell subsets (GEO accession no. GSE114631). NES, normalized enrichment score; FDR, false discovery rate q-value. **(D)** Heatmaps illustrating the relative expression of signature genes in WT and *Stat3*$^{-/-}$ OT-I TILs. **(E)** Lists of top 15 Gene Ontology (GO) biological pathways for DEGs of WT and *Stat3*$^{-/-}$ OT-I TILs. P value presented as $-\log_{10}{}^{(P\ value)}$. Columns designate $-\log_{10}{}^{(P\ value)}$ and circles designate gene ratio (%). **(F)** Representative plots (left panel) and quantification (right panel) of Granzyme B production level in TIM-3⁻ T_{ex}^{prog} and TIM-3⁺ T_{ex}^{term} OT-I cells from B16-OVA tumors. **(G)** Representative plots (left panel) and quantifications (right panel) of TCF1 and Granzyme B expression in splenic OT-I cells on day 8 after LM-OVA infection. **(H)** Absolute frequencies of TCF1⁺ and Granzyme B⁺ OT-I cells in the spleen, which were the product of OT-I cell frequencies and TCF1⁺ or Granzyme B⁺ cell ratios. Data are representative of two (G and H) or three (A–C and F) independent experiments. Data are shown as mean ± SEM. *, P < 0.05; **, P < 0.01; ***, P < 0.001; ****, P < 0.0001 by paired two-tailed Student's *t* test (A and F–H).

short-lived effector CD8⁺ T cells were reduced and those of CD127⁺KLRG1⁻ memory precursors were increased in the deficiency of *Stat3* (Fig. S2 L). Moreover, the expression levels of Granzyme B in TCF1⁻Granzyme B⁺ *Stat3*$^{-/-}$ OT-I cells were also significantly reduced (Fig. S2 M). These results support the essential role of *Stat3* in the development of cytolytic effector CD8⁺ T cells. Consistently, *Stat3* deficiency resulted in lower percentages of OT-I cells in the spleen, and both TCF1⁺Granzyme B⁻ and TCF1⁻Granzyme B⁺ OT-I cell numbers were decreased by *Stat3* deletion (Fig. 2 H and Fig. S2 N). However, the proliferation of OT-I cells was unaffected in the absence of *Stat3* as indicated by the similar percentages of Ki-67–expressing cells (Fig. S2 O).

These results altogether indicated that STAT3 played critical roles in regulating the differentiation, survival, and function of CD8⁺ T cells in cancer and acute infection, especially in favoring

terminally differentiated CD8⁺ T cell fitness and effector functions.

IL-10 and IL-21 promote STAT3 activation in T_{ex}^{term} cells in cancer

Multiple STAT3-activating cytokines have been implicated in tumor immunity (Cui et al., 2021; Guo et al., 2021; Hanna et al., 2021; Yu et al., 2014; Yu et al., 2009). Thus, to identify the upstream extracellular inducers for STAT3 activation within tumor-infiltrating CD8⁺ T cells, we first analyzed the expression of receptors for its canonical inducing cytokines in CD8⁺ TILs from public single-cell datasets of human cancer patients (Guo et al., 2018; Zhang et al., 2018; Zheng et al., 2017). We found that IL-10 receptors (*IL10RA* and *IL10RB*) were highly expressed in tumor-infiltrating CD8⁺ T cells in lung cancer, CRC, and HCC patients (Fig. 3 A). *IL21R* expression was also elevated in PD-1⁺ CD8⁺ TILs as compared with peripheral CD8⁺ T cells (Fig. 3 A). However, *IL6RA* was barely expressed in CD8⁺ TILs in lung cancer and CRC patients although high mRNA levels of *IL6ST* (encoding GP130) were found in CD8⁺ TILs (Fig. 3 A). In addition, *IL23R* and *S1PR1* were also almost not expressed in tumor-infiltrating CD8⁺ T cells (Fig. 3 A). Moreover, although leptin was reported to regulate CD8⁺ T cells via STAT3 signaling in murine breast cancer (Zhang et al., 2020), its receptor was hardly expressed in CD8⁺ TILs in human lung cancer, CRC, and HCC patients at the mRNA level (Fig. 3 A). In addition, growth factor receptors, GPCRs, TLRs, and CSF receptors also had limited mRNA expression in tumor-infiltrating CD8⁺ T cells (data not shown). Thus, IL-10 and IL-21 might be two candidate upstream inducers for STAT3 activation in CD8⁺ TILs within human tumors.

Next, we further examine the ability of IL-10 and IL-21 in inducing STAT3 phosphorylation and activation in murine tumor-infiltrating CD8⁺ T cells. Consistent with the above human T cell data, IL-10 and IL-21, but not IL-6, induced STAT3 phosphorylation at both Tyr705 (pY705) and Ser727 (pS727) sites in CD8⁺ TILs from both B16-OVA and E.G7 tumors (Fig. 3, B and C). Importantly, pY705 levels in CD8⁺ TILs were much higher than those in CD44⁻ and CD44⁺ CD8⁺ T cells from TDLNs (Fig. 3 B), consistent with elevated STAT3 expression in CD8⁺ TILs mentioned above (Fig. S1, B and C). In addition, though IL-6 failed to induce pSTAT3 in tumor-infiltrating T_{ex} cells, it potently induced STAT3 phosphorylation in CD44⁻ and CD44⁺ CD8⁺ T cells from TDLNs, while IL-10 was not able to induce pSTAT3 in naive CD8⁺ T cells (Fig. 3 B). The differential abilities of IL-6 and IL-10 to induce pSTAT3 were consistent with the expression of their receptors. IL-6Rα expression was highly enriched in naive CD8⁺ T cells but was downregulated during activation and was diminished in T_{ex} cells within tumors (Fig. 3 D; Yang et al., 2016). Conversely, IL10RA expression was gradually upregulated in CD8⁺ T cells during activation and differentiation and highly expressed in tumor-infiltrating CD8⁺ T cells (Fig. 3 D; Emmerich et al., 2012).

We further compared the phosphorylated levels of STAT3 in T_{ex}^{prog} and T_{ex}^{term} subsets and found that IL-10 and IL-21 induced relatively higher levels of pSTAT3 at both Y705 and S727 sites in T_{ex}^{term} cells as compared with those in T_{ex}^{prog} cells from B16-OVA and E.G7 tumors (Fig. 3 E), which was consistent with higher *Stat3* expression in *Pdcd1*^{hi}*Havcr2*⁺ CD8⁺ TILs than in *Pdcd1*^{hi}*Havcr2*⁻ CD8⁺ TILs observed from single-cell data of B16-OVA–infiltrated CD8⁺ T cells (Fig. 3 F). Consistently, the mRNA level of *STAT3* was also increased in *PDCD1*^{hi}*HAVCR2*^{hi} CD8⁺ TILs as compared with that in *PDCD1*^{hi}*HAVCR2*^{low} CD8⁺ TILs in human lung cancer, CRC, and HCC patients (Fig. 3 G). These results suggest that STAT3 signaling might more preferentially regulate T_{ex}^{term} TILs, consistent with the above results on the potent regulation of T_{ex}^{term} cell maintenance and effector function by STAT3 (Fig. 2, A and F).

IL-10 and IL-21 signaling intrinsically promotes the development of T_{ex}^{term} cells

Next, to understand the activation of STAT3 signaling in CD8⁺ TILs, we functionally analyzed and compared the roles of IL-10 and IL-21 signaling. We stimulated in vitro–activated WT and *Stat3*-deficient CD8⁺ T cells with IL-10 or IL-21 for another 3 d, with IL-6 as the control (Fig. 4 A). Results showed that IL-10 and IL-21 significantly induced the generation of CD25^{hi}TIM-3⁺ subsets in vitro as compared with unstimulated control, while TCF1 expression was dramatically decreased by the stimulation of both IL-10 and IL-21 (Fig. 4, B–D). Importantly, IL-10 failed in inducing the generation of CD25^{hi}TIM-3⁺ population in *Stat3*$^{-/-}$ CD8⁺ T cells, indicating that the induction of CD25^{hi}TIM-3⁺ cells by IL-10 was STAT3-dependent (Fig. 4, C and D). IL-21 induced increased frequencies of CD25^{hi}TIM-3⁺ cells in WT CD8⁺ T cells than in *Stat3*$^{-/-}$ CD8⁺ T cells, with a great portion of CD25^{hi}TIM-3⁺ cells found in *Stat3*-deficient CD8⁺ T cells (Fig. 4, C and D), indicating that IL-21 inducing TIM-3⁺ cell development partially, not totally, relied on STAT3 signaling, which might be due to IL-21 activation of STAT1 and STAT5 in addition to STAT3 signaling in CD8⁺ T cells (Delgoffe and Vignali, 2013; Mujib et al., 2012). It should also be noticed that IL-21 induced a much higher percentage of CD25^{hi}TIM-3⁺ cells than IL-10 or IL-6, and TCF1⁺ cell percentages were also reduced the most in IL-21–stimulated CD8⁺ T cells (Fig. 4, B–D), associated with higher pSTAT3 levels following IL-21 treatment of in vitro–activated CD8⁺ T cells as compared with IL-6 and IL-10 treatment (Fig. S3 A). IL-6 had limited effects in promoting CD25^{hi}TIM-3⁺ cell development or inhibiting TCF1 expression in activated CD8⁺ T cells (Fig. 4, B–D), perhaps due to dramatically downregulated IL6-Rα expression in the process of priming, with little or no expression in CD8⁺ T cells activated in vitro (Yang et al., 2016). Moreover, the expression of CD25 and CD39 was significantly upregulated, while that of Ly108 and CD62L was downregulated in WT CD8⁺ T cells exposed to IL-10 and IL-21 as compared with unstimulated control or *Stat3*$^{-/-}$ CD8⁺ T cells (Fig. S3, B and C). These results suggest that the IL-10/21–STAT3 axis plays critical roles in promoting T_{ex}^{term} cell generation after activation.

Next, to further explore whether the IL-10/21–STAT3 axis regulated CD8⁺ T cell differentiation via an intrinsic and direct way, we cocultured naive WT and *Stat3*$^{-/-}$ CD8⁺ T cells in vitro and stimulated them with cytokines for another 3 d after activation. We found in the coculture system that IL-10 and IL-21 significantly induced CD25^{hi}TIM-3⁺ cell generation and inhibited TCF1 expression in WT, but less in cocultured *Stat3*$^{-/-}$

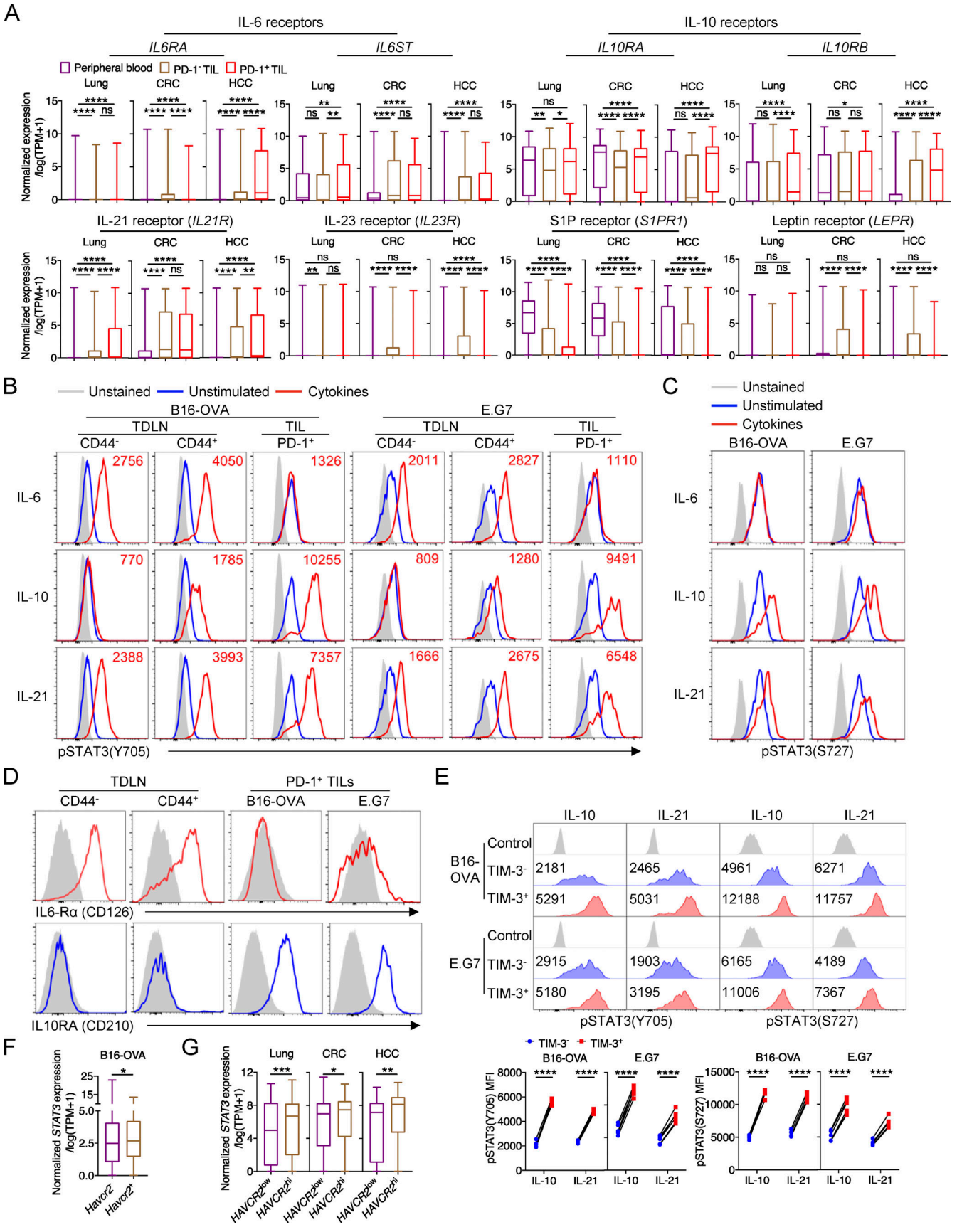

Figure 3. **IL-10 and IL-21 promote STAT3 activation in T_{ex}^{term} cells in cancer. (A)** mRNA levels of cytokine receptors in CD8⁺ T cells from peripheral blood and tumors in human cancer patients (GEO accession nos. GSE99254, GSE108989, and GSE98638). **(B)** Representative plots of phosphorylated STAT3 at the

Y705 site in CD8⁺ T cells from TDLNs and B16-OVA tumors (left panel) or E.G7 tumors (right panel). Cells were stimulated by IL-6, IL-10, or IL-21 for 30 min in vitro. **(C)** Representative plots of phosphorylated STAT3 at the S727 site in CD8⁺ T cells from B16-OVA (left panel) and E.G7 (right panel) tumors. Cells were stimulated by IL-6, IL-10, or IL-21 for 30 min in vitro. **(D)** IL6-Rα (CD126) and IL10RA (CD210) expression on CD8⁺ T cells from TDLNs and tumors. **(E)** Representative plots (upper panel) and quantifications (bottom panel) of pSTAT3(Y705) and pSTAT3(S727) in PD-1⁺TIM-3⁻ and PD-1⁺TIM-3⁺ CD8⁺ TILs from B16-OVA (left panel) or E.G7 (right panel) tumors. Cells were stimulated by IL-10 or IL-21 for 30 min in vitro. **(F)** mRNA level of *Stat3* in *Pdcd1*^{hi}*Havcr2*$^{-}$ and *Pdcd1*^{hi}*Havcr2*$^{+}$ CD8⁺ T cells from B16-OVA tumors (GEO accession no. GSE122675). *Pdcd1*^{hi}, *Pdcd1* expression value >1; *Havcr2*$^{+}$, *Havcr2* expression value >0; *Havcr2*$^{-}$, *Havcr2* expression value = 0. **(G)** mRNA level of *STAT3* in *PDCD1*^{hi}*HAVCR2*^{low} and *PDCD1*^{hi}*HAVCR2*^{hi} CD8⁺ T cells from tumors in human cancer patients (GEO accesssion nos. GSE99254, GSE108989, and GSE98638). *PDCD1*^{hi}, *PDCD1* expression value >5; *PDCD1*^{hi} cells were ranked by *HAVCR2* expression value, top 50% are *HAVCR2*^{hi}, and the other 50% are *HAVCR2*^{low}. Data are representative of three (B–D) or two (E) independent experiments. Data are shown as mean ± SEM. *, P < 0.05; **, P < 0.01; ***, P < 0.001; ****, P < 0.0001 by one-way ANOVA (A), paired two-tailed Student's *t* test (E) and unpaired two-tailed Student's *t* test (F and G).

CD8⁺ T cells and unstimulated CD8⁺ T cells (Fig. S3, D–F). These data indicated that the function of IL-10 and IL-21 in *Stat3*-deficient CD8⁺ T cells could not be rescued by the factors in the supernatant of IL-10/21–treated WT CD8⁺ T cells. Hence, the IL-10/21–STAT3 axis intrinsically regulates CD8⁺ T cell fate decision after activation.

Moreover, IL-10/21 signaling significantly promoted Granzyme B expression in activated WT CD8⁺ T cells as compared with *Stat3*$^{-/-}$ CD8⁺ T cells and unstimulated control (Fig. 4 E). To further assess the function of STAT3 in the regulation of CD8⁺ T cell killing on targeted tumor cells, we used IL-10 to activate STAT3 in OT-I cells primed in vitro for 3 d, then performed a killing assay with B16-OVA tumor cells as targets. IL-10–stimulated WT OT-I cells had a greater cytolytic capacity for tumor cells than IL-10–treated *Stat3*$^{-/-}$ OT-I cells and unstimulated control (Fig. 4 F), indicating that active STAT3 signaling could efficiently enhance CD8⁺ T cell–mediated tumor killing. In addition, we found IL-10/21 signaling dramatically enhanced the proportion of viable cells in WT CD8⁺ T cells in vitro, resulting in greater numbers of live CD8⁺ T cells as compared with *Stat3*$^{-/-}$ CD8⁺ T cells and unstimulated control (Fig. 4, G and H), indicating a critical role of STAT3 in promoting CD8⁺ T cell survival. However, IL-10/21–STAT3 axis did not enhance the proliferative activity of activated CD8⁺ T cells, illustrated by CellTrace Violet (CTV) dilution, in IL-10– and IL-21–stimulated WT and *Stat3*$^{-/-}$ CD8⁺ T cells (Fig. S3 G).

In vivo, by analyzing cotransferred WT and *Il10ra*$^{-/-}$ OT-I cells within B16-OVA tumors, we found the frequencies of Ly108^{-}TIM-3^{+} T_{ex}^{term} cells were decreased by the deficiency of *Il10r* as previously reported, while the percentages of Ly108^{+}TIM-3^{-} T_{ex}^{prog} cells were increased (Fig. S3, H–J). IL-10-Fc was shown to further expand tumor-specific TIM-3^{+} cells in B16F10 tumors (Guo et al., 2021), which was consistent with the results obtained in vivo by the deletion of *Stat3*. Moreover, *Il21r* deficiency impaired the differentiation and function of cytolytic T_{ex} cells in B16F10 and KP-HELLO solid tumor models (Cui et al., 2021; Zander et al., 2019), which was also consistent with the results of *Stat3*-deficiency. In contrast, *Il6ra* deficiency in activated OT-I cells did not affect the development of T_{ex}^{term} vs. T_{ex}^{prog} cells within tumors as expected (Fig. S3, H and K).

To further comprehensively analyze the functional relationships between IL-10- and IL-21–STAT3 signaling, we compared the RNA-seq data of WT and *Stat3*$^{-/-}$ OT-I cells from B16-OVA tumors (Fig. S2 G) with previously reported RNA-seq results of tumor-specific PD-1⁺TIM-3⁺ CD8⁺ TILs from IL-10-Fc–treated B16F10-bearing mice (Guo et al., 2021) and in vitro IL-21–stimulated activated CD8⁺ T cells (Hermans et al., 2020). GSEA results revealed that both IL-10-Fc– and IL-21–induced signature genes were relatively enriched in tumor-infiltrating WT T_{ex} cells, while their suppressed feature genes were significantly concentrated in *Stat3*$^{-/-}$ CD8⁺ TILs (Fig. 4 I). In addition, both IL-10-Fc– and IL-21–stimulated CD8⁺ T cells were more similar to T_{ex}^{term} cells in their gene expression, while their inhibited genes were relatively more enriched in T_{ex}^{prog} cells (Fig. 4 I; Siddiqui et al., 2019). Moreover, by overlapping IL-10-Fc– and STAT3-regulated genes, we found their regulated genes were significantly correlated (Fig. 4 J). Specifically, IL-10 upregulated the expression of numerous T_{ex}^{term}-related genes (*Id2*, *Entpd1*, *Gzmb*, etc.) as STAT3 did, while it inhibited the expression of multiple T_{ex}^{prog}-related genes (*Ccr7*, *Slamf6*, etc.), which were simultaneously repressed by STAT3 (Fig. 4 J). IL-21 and STAT3 also had identical functions in promoting the expression of T_{ex}^{term}-related genes (*Id2*, *Havcr2*, *Gzmb*, etc.) and in suppressing those of T_{ex}^{prog}-related genes (*Tcf7*, *Id3*, *Cxcr5*, etc.; Fig. 4 K).

These results, therefore, indicate that IL-10 and IL-21 are two inducers of STAT3 activation, and thereby regulate T_{ex} cells within tumors. STAT3 signaling not only plays critical roles in promoting T_{ex}^{term} cell maintenance but is also essential for T_{ex}^{term} cell development.

STAT3 transcriptionally regulates T_{ex} cell differentiation

To systematically understand the transcriptional mechanisms whereby STAT3 regulates CD8⁺ T cell differentiation, we further analyzed the genome-wide occupancy of phosphorylated STAT3 in activated CD8⁺ T cells. Since pY705 was predominantly responsible for the nuclear translocation of STAT3 dimer and the binding to DNA consensus sequence (Huynh et al., 2019), we performed chromatin immunoprecipitation coupled with high-throughput sequencing (ChIP-seq) analysis using in vitro activated CD8⁺ T cells stimulated by IL-6, IL-10, or IL-21 to induce phosphorylation at Y705. Results showed that IL-6–, IL-10–, and IL-21–induced pSTAT3 significantly bound to 3,987, 7,113, and 9,549 genomic sites, respectively (Fig. 5, A and B; and Table S2). Almost all sites occupied by pSTAT3 induced by IL-6 and IL-10 were also bound by pSTAT3 induced by IL-21 (Fig. 5 A). Stronger binding signals could be detected in IL-6–, IL-10–, and IL-21–induced pSTAT3 cobinding sites as compared with their own unshared binding sites (Fig. S4 A). Thus, IL-6/10/21–induced pSTAT3 bound to a shared genomic profile, and the

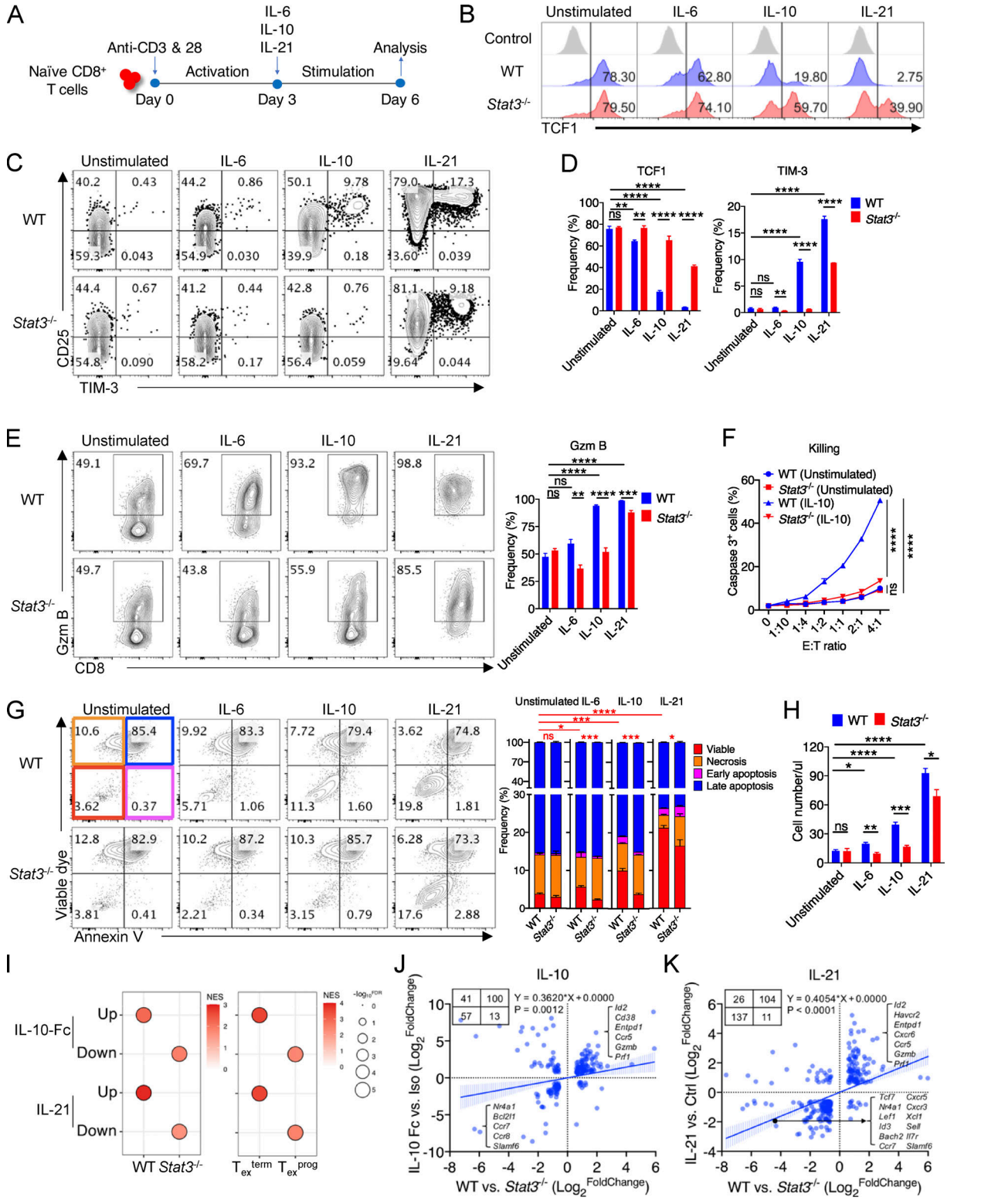

Figure 4. **IL-10 and IL-21 signaling intrinsically promotes the development of T_{ex}^{term} cells. (A)** Experimental design for in vitro culture of WT and *Stat3*$^{-/-}$ CD8$^+$ T cells with the stimulation of IL-6, IL-10, or IL-21. **(B–D)** Representative plots (B and C) and quantifications (D) of TCF1 and TIM-3 expression in/on in vitro–stimulated WT and *Stat3*$^{-/-}$ CD8$^+$ T cells (n = 4 in each group). **(E)** Representative plots (left panel) and quantification (right panel) of Granzyme B production in in vitro–stimulated WT and *Stat3*$^{-/-}$ CD8$^+$ T cells (n = 4 in each group). **(F)** Killing assay of WT and *Stat3*$^{-/-}$ OT-I cells to B16-OVA tumor cells indicated by intracellular cleaved caspase 3 (n = 3 in each group). Activated CD8$^+$ T cells were stimulated with IL-10 for 3 d or not. **(G)** Representative plots (left panel) and quantifications (right panel) of viable dye and Annexin V staining on in vitro–stimulated WT and *Stat3*$^{-/-}$ CD8$^+$ T cells (n = 4 in each group). **(H)** Numbers of in vitro–stimulated WT and *Stat3*$^{-/-}$ CD8$^+$ T cells (n = 4 in each group). **(I)** GSEA results for comparing the enrichment of IL-10-Fc– or IL-21–regulated feature genes in the transcriptomes of WT and *Stat3*$^{-/-}$ OT-I TILs (left panel), or T_{ex}^{term} and T_{ex}^{prog} cells (right panel) (GEO accession nos.

GSE168990, GSE143903, and GSE114631). NES, normalized enrichment score; FDR, false discovery rate q-value. FDR presented as $-\log_{10}^{(FDR)}$. **(J)** Correlation analysis for DEGs identified in IL-10-Fc– and STAT3-relevant RNA-seq (GEO accession no. GSE168990). DEGs were filtered by fold change >1.5 and P value <0.05. **(K)** Correlation analysis for DEGs identified in IL-21– and STAT3-relevant RNA-seq (GEO accession no. GSE143903). DEGs were filtered by fold change >1.5 and P value <0.05. Data are representative of three (B–E and H) or two (F and G) independent experiments. Data are shown as mean ± SEM. *, P < 0.05; **, P < 0.01; ***, P < 0.001; ****, P < 0.0001 by unpaired two-tailed Student's *t* test (D, E, G, and H) and two-way ANOVA (F).

binding affinities in activated CD8⁺ T cells correlated with the pSTAT3 levels induced by these three cytokines (Fig. S3 A and Fig. S4 A). Consistently, genes bound by IL-6/10/21–induced pSTAT3 were significantly enriched in biological pathways related to T cell differentiation, T cell receptor signaling, cytotoxicity, and other immunological pathways (Fig. S4 B).

Further analyses revealed that pSTAT3-binding sites were mainly distributed in the distal intergenic, intron, and promoter regions (Fig. 5 B), and above 38% of binding sites fell into 10–50 kb upstream or downstream of the transcription start sites (TSS), with another 13–17% and 11–13% binding sites located at 0–1 and 50–100 kb away from TSS, respectively (Fig. 5 B). Consistently, density maps and peak plots showed that extensive H3K27ac and H3K4me1 modifications, markers for actively transcribed regions and enhancers, respectively (Kurachi et al., 2014), were localized within ±10 kb regions centered around pSTAT3-binding sites (Fig. S4 C). These results indicated that pSTAT3 mostly bound to enhancers or other distal regulatory elements to regulate gene transcription, consistent with its role in shaping active enhancer landscape found in CD4⁺ T cells (Vahedi et al., 2012), while another major portion of STAT3 binding was also in promoter and intron regions.

To identify pSTAT3-regulated genes in tumor-specific T_{ex} cells, we integrated pSTAT3 ChIP-seq data with RNA-seq data of WT and *Stat3*$^{-/-}$ OT-I TILs and got STAT3-induced and STAT3-suppressed genes (Fig. 5 C, Fig. S2 G, Fig. S4 D, and Table S2). To pinpoint STAT3-regulated genes that were directly involved in tumor-infiltrating T_{ex} cell fate decision, we overlapped STAT3-regulated genes with the signature genes of tumor-specific TCF1⁺ T_{ex}^{prog} or TCF1⁻ T_{ex}^{term} cells from B16-OVA tumors, respectively (Siddiqui et al., 2019). Interestingly, numerous STAT3-induced genes were identified as T_{ex}^{term} signature genes, including *Id2*, *Havcr2*, *Entpd1*, *Gzmb*, and *Cxcr6*, whereas T_{ex}^{prog} feature genes were not found (Fig. 5, D and E). Moreover, a broad range of T_{ex}^{prog} signature genes (*Tcf7*, *Id3*, *Sell*, *Btla*, *Cxcr5*, *Ccr7*, etc.) were directly inhibited by STAT3 while none of the T_{ex}^{term} feature genes were suppressively bound by STAT3 (Fig. 5, D and E). Consistently, GSEA results revealed that IL-6–, IL-10–, and IL-21-STAT3–induced genes were all relatively enriched in TCF1⁻ T_{ex}^{term} subset, while their inhibited genes were significantly concentrated in the TCF1⁺ T_{ex}^{prog} subset (Fig. S4 E). To investigate the relevance of STAT3-regulated genes in tumor-infiltrating CD8⁺ T cells from human cancers, we utilized published scRNA-seq data from human head and neck cancer and melanoma patients (Puram et al., 2017; Sade-Feldman et al., 2018). A memory-like CD8⁺ T cell subset was identified with higher expression of memory hallmark genes such as *TCF7*, *IL7R*, and *CCR7* (Fig. 5 F and Fig. S4 F). Another subset showed high-level transcripts of effector and cytotoxicity signature genes, including *GZMB*, *HAVCR2*, and *PRDM1*, and thus was identified as a cytolytic subset (Fig. 5 F and Fig. S4 F). In line with the above murine data, STAT3-induced genes showed higher transcript expression in the cytolytic subset in both human head and neck cancer and melanoma patients (Fig. 5 G and Table S3). Altogether, these results indicated the potent transcriptional functions of STAT3 signaling in regulating T_{ex} cell differentiation, especially in promoting effective T_{ex}^{term} cell development.

To further analyze the specific occupancy of pSTAT3 on open chromatin regions (OCRs) of its target genes in tumor-infiltrating CD8⁺ T cells, we aligned pSTAT3 ChIP-seq tracks with transposase-accessible chromatin with high-throughput sequencing (ATAC-seq) tracks of OVA-specific T_{ex}^{term} and T_{ex}^{prog} cells from B16-OVA tumors (Miller et al., 2019), as well as RNA-seq tracks of the above mentioned WT and *Stat3*$^{-/-}$ OT-I cells from B16-OVA tumors. We found that pSTAT3 occupied the promoter regions of multiple T_{ex}^{term}-related genes, including *Id2*, *Batf*, *Gzmb*, and *Prf1*, which might lead to their enhanced transcriptional activities (Fig. 5 H and Fig. S4 G). Also pSTAT3 occupied the promoters of T_{ex}^{prog}-related genes, including *Cxcr5* and *Il7r*, accompanied by their reduced transcripts (Fig. 5 H and Fig. S4 G). Moreover, pSTAT3 was found to directly bind to multiple distal intergenic regions of T_{ex}^{prog}-associated genes, including *Id3*, *Tcf7*, *Ccr7*, *Cxcr5*, and *Il7r* along with decreased transcriptional activities (Fig. 5 H and Fig. S4 G). In addition, pSTAT3 also inductively bound to the introns of *Havcr2* and *Prdm1* genes, and suppressively bound to those of *Ccr7*, *Bach2*, and *Sell* genes, and these loci were all accessible in tumor-specific T_{ex} cells (Fig. 5 H and Fig. S4 G).

To further confirm the transcriptional regulation of STAT3 on the identified target genes, we used IL-10 to activate STAT3 signaling in CD8⁺ T cells primed in vitro and then analyzed their mRNA levels. We found that *Id2* and *Gzmb* expressions were dramatically upregulated in IL-10–stimulated WT CD8⁺ T cells as compared with IL-10–stimulated *Stat3*$^{-/-}$ CD8⁺ T cells and unstimulated control (Fig. 5 I). In the meantime, *Id3* and *Ccr7* expressions were significantly downregulated by IL-10 in WT CD8⁺ T cells, as expected (Fig. 5 I).

Thus, these results demonstrate that STAT3 signaling promotes T_{ex}^{term} cell differentiation via transcriptionally upregulating the expression of their signature genes, including *Id2*, *Havcr2*, *Gzmb*, etc. In the meantime, STAT3 also inhibits T_{ex}^{prog} cell fate commitment by directly suppressing the expression of their fate-associated genes, including *Id3*, *Ccr7*, *Tcf7*, etc. It should be noticed that although IL-6 transiently induces STAT3 activation in CD8⁺ T cells in vitro, it fails in constantly regulating CD8⁺ T cell differentiation via STAT3 signaling after activation due to the diminishing IL6-Rα expression (Fig. 4, B–D; Yang et al., 2016).

STAT3 regulates the epigenetic landscape of T_{ex} cells in cancer

Since T_{ex} cells exhibit specific epigenetic landscapes (Miller et al., 2019), we further explored whether STAT3 has a

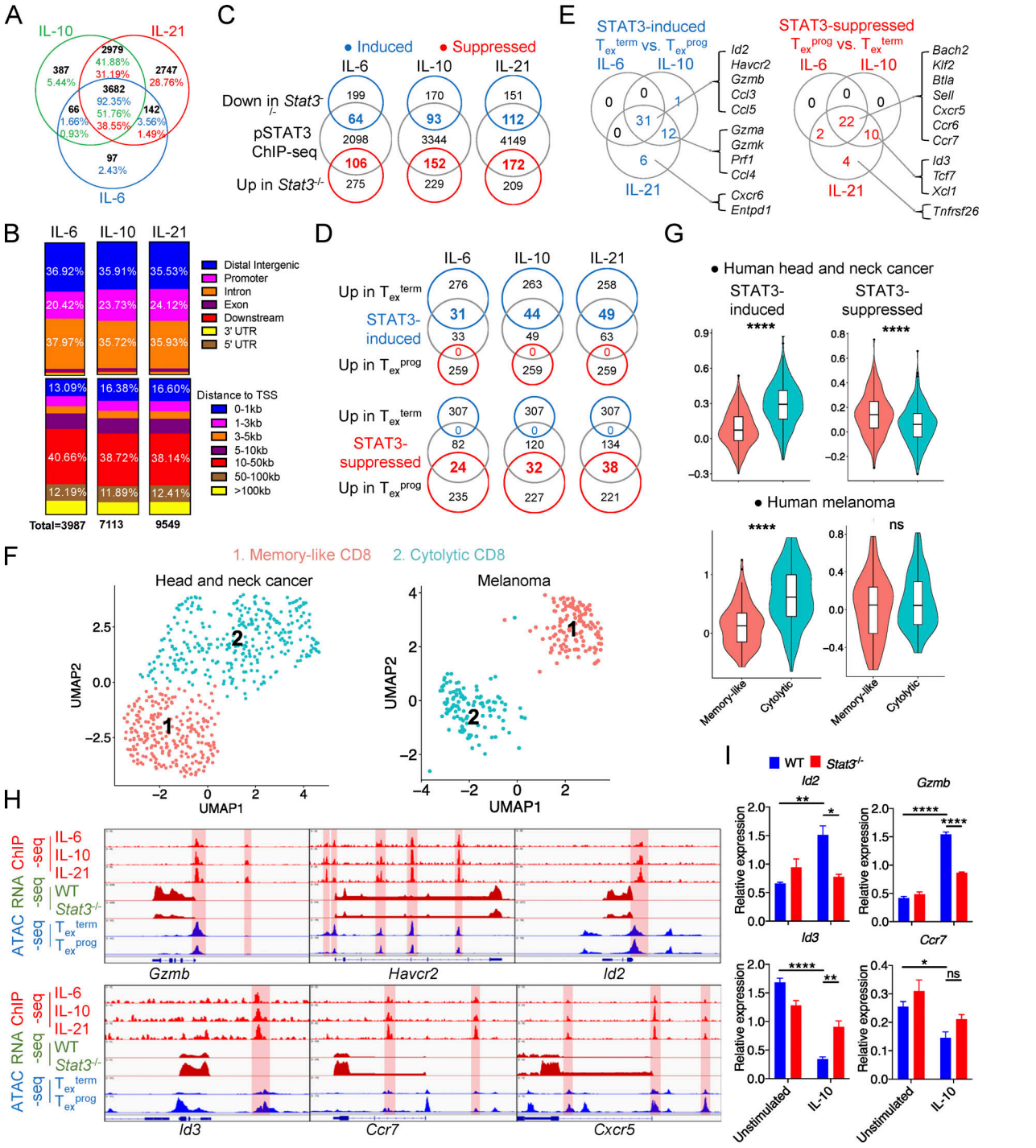

Figure 5. **STAT3 transcriptionally regulates T_{ex} cell differentiation. (A)** Venn diagram of pSTAT3-binding peaks in IL-6–, IL-10–, and IL-21–stimulated CD8⁺ T cells across the whole mouse genome (mm10). **(B)** Genetic feature distribution (upper panel) or distribution relative to TSS (bottom panel) of pSTAT3-binding peaks in CD8⁺ T cells. **(C)** Venn diagrams of pSTAT3-binding genes and DEGs in WT or *Stat3*$^{-/-}$ CD8⁺ OT-I TILs. **(D)** Venn diagrams of STAT3-regulated genes and DEGs in T_{ex}^{term} or T_{ex}^{prog} TILs (GEO accession no. GSE114631). **(E)** Representative STAT3-regulated feature genes of T_{ex}^{term} (left panel) or T_{ex}^{prog} (right panel) cells. **(F)** UMAP plots identifying tumor-infiltrating memory-like and cytolytic CD8⁺ T cell clusters from human head and neck cancer (left panel) or melanoma (right panel) patient (GEO accession nos. GSE103322 and GSE120575). **(G)** Average expression of STAT3-induced (left panel) or -suppressed (right panel) signature gene clusters in memory-like or cytolytic tumor-infiltrating CD8⁺ T cells. STAT3-induced or -suppressed signature genes are listed in Table S3. **(H)** pSTAT3 ChIP-seq tracks aligned with RNA-seq tracks of WT and *Stat3*$^{-/-}$ CD8⁺ TILs, and ATAC-seq tracks of T_{ex}^{prog} or T_{ex}^{term} cells at the specific gene loci (GEO accession no. GSE123236). **(I)** mRNA levels of specific genes in in vitro activated WT and *Stat3*$^{-/-}$ CD8⁺ T cells with the stimulation of IL-10 for 2 d or not. Data are representative of three (I) independent experiments. Data are shown as mean ± SEM. *, P < 0.05; **, P < 0.01; ***, P < 0.001; ****, P < 0.0001 by unpaired two-tailed Student's *t* test (G and I).

function in regulating the chromatin accessibilities of T_{ex} cells using ATAC-seq on cotransferred WT and *Stat3*$^{-/-}$ OT-I cells from B16-OVA tumors (Fig. 1 D). Results showed that the chromatin accessibilities of T_{ex} cells were globally reduced by the deficiency of *Stat3* (Fig. 6 A). 1,253 OCRs had reduced accessibilities across the whole genome in *Stat3*$^{-/-}$ OT-I TILs, with only 71 OCRs showing increased accessibilities in *Stat3*$^{-/-}$ OT-I TILs (Fig. 6 A and Table S4), suggesting a critical role of STAT3 mainly in activating the chromatin accessibility of CD8$^+$ T cells during T cell exhaustion in cancer. The altered OCRs were mainly distributed in the promoter, distal intergenic, and intron regions (Fig. 6 B), and mainly located at 0–1 kb and 10–50 kb distance from TSS (Fig. 6 C).

To further investigate the regulation of STAT3 on the chromatin structures of T_{ex}^{term} or T_{ex}^{prog} signature genes, we compared the accessibilities of the differentially accessible peaks (DA peaks) in WT and *Stat3*$^{-/-}$ T cells (Miller et al., 2019). We found that the overall accessibilities of both T_{ex}^{term} and T_{ex}^{prog} DA peaks were reduced in *Stat3*$^{-/-}$ T_{ex} cells as compared with WT T_{ex} cells (Fig. 6 D). To further illustrate the epigenetic regulation by STAT3, we also analyzed the genome-wide profiling of H3K27ac modification in in vitro IL-10–stimulated WT and *Stat3*$^{-/-}$ CD8$^+$ T cells. Consistent with ATAC-seq results, the H3K27ac modification was globally reduced in IL-10–stimulated *Stat3*$^{-/-}$ CD8$^+$ T cells as compared with IL-10–stimulated WT CD8$^+$ T cells (Fig. 6 E and Table S5). Moreover, *Stat3* deficiency decreased H3K27ac modification profiling around both the T_{ex}^{term} and T_{ex}^{prog} DA Peaks (Fig. 6 F). Importantly, peak set enrichment analysis (PSEA) results revealed that the epigenetic signatures of T_{ex}^{term} and effector CD8$^+$ T cells were strongly enriched in WT OT-I TILs, while signature OCRs in T_{ex}^{prog} and memory CD8$^+$ T cells were significantly concentrated in *Stat3*$^{-/-}$ OT-I TILs (Fig. 6 G). Thus, these results indicated that STAT3 exerted a critical function in the epigenetic regulation of T_{ex} cell chromatin profiles, especially in favoring T_{ex}^{term} epigenetic program. Moreover, the feature OCRs with reduced accessibilities in anti-IL-10R–treated PD-1^{hi} CD8$^+$ T cells in the leukemia model (Hanna et al., 2021) were relatively enriched in WT CD8$^+$ T cells, while those with increased accessibilities were significantly associated with *Stat3*$^{-/-}$ CD8$^+$ T cells (Fig. 6 H), revealing the identical role of IL-10 and STAT3.

Moreover, we found that H3K27ac modification profiling around TSS in *Stat3*$^{-/-}$ CD8$^+$ T cells declined as compared with that in WT CD8$^+$ T cells (Fig. 6 I), and the chromatin accessibilities and H3K27ac modifications around pSTAT3-binding peaks were also significantly reduced as a result of *Stat3* deficiency (Fig. 6, J and K), indicating that the STAT3 binding to target gene loci might be critical for the openness and transcriptional activation in these sites.

STAT3 cooperates with BATF and IRF4 to mediate T_{ex}^{term} cell development

In addition to the above results, known motif enrichment analyses for STAT3-regulated OCRs revealed that *Stat3* deficiency resulted in decreased enrichment for binding motifs of numerous AP-1, ETS, and RUNX family members (Fig. 7 A). Moreover, plenty of STAT, AP-1, ETS, and RUNX family members were also significantly enriched in pSTAT3-occupied peaks (Fig. S5 A). These indicated that there might exist significant crosstalk between STAT3 and other transcription factors. AP-1 transcription factors play critical roles in T cell activation, differentiation, and exhaustion (Philip and Schietinger, 2021). To further explore the relationships between STAT3 and AP-1 family members, we compared their binding profiles in detail using previously published datasets (Kurachi et al., 2014). Density maps and peak plots revealed that a great deal of AP-1–occupied peaks was shared with pSTAT3-binding sites around the genome, especially BATF and IRF4 (Fig. S5 B), and compared with TCF1 and T-bet binding, that of BATF and IRF4 was significantly enriched at pSTAT3-occupied sites (Fig. 7 B). Moreover, increased pSTAT3 occupancy was found at genomic sites cobound by BATF or IRF4 or both as compared with pSTAT3 unshared binding sites (Fig. 7 C). Similarly, greater binding signals of BATF or IRF4 were also detected in their cobinding sites with pSTAT3 than in their own unshared occupied peaks (Fig. S5, C and D). Importantly, the overall chromatin accessibilities and H3K27ac modifications located at BATF- or IRF4-occupied sites were significantly reduced in *Stat3*$^{-/-}$ T_{ex} cells (Fig. 7, D and E; and Fig. S5 E).

BATF and IRF4 have been demonstrated to play vital roles in promoting the expansion and cytolytic function of exhausted effector CD8$^+$ T cells in chronic infection and cancer (Chen et al., 2021; Man et al., 2017; Seo et al., 2021; Xin et al., 2015), and STAT3 could directly promote BATF expression in CD8$^+$ T cells (Fig. 2 D and Fig. S4 G; Xin et al., 2015). To further explore the functional relationships between STAT3 and BATF or IRF4 in CD8$^+$ T cells during their exhaustion, we next compared their regulated transcriptomes. GSEA results revealed that both BATF- and IRF4-induced signature genes were significantly enriched in WT TILs, while their inhibited genes were relatively concentrated in *Stat3*$^{-/-}$ TILs (Fig. 7 F; Man et al., 2017; Seo et al., 2021). By overlapping their regulated genes identified from their RNA-seq data, we found that a set of T_{ex}^{term} feature genes (*Entpd1*, *Gzmb*, *Havcr2*, *Cxcr6*, etc.) were coupregulated by STAT3 and BATF, or by STAT3 and IRF4 (Fig. S5, F and G), and multiple T_{ex}^{prog} signature genes (*Id3*, *Ccr7*, *Tcf7*, *Slamf6*, etc.) were downregulated jointly by STAT3 and BATF or IRF4 (Fig. S5, F and G). This implied that the function of STAT3 in regulating T_{ex} cell differentiation might be in collaboration with BATF or IRF4. To further explore the transcriptional program coordinated by these three factors, we overlapped their binding genes identified from their ChIP-seq data and found they co-occupied to numerous gene loci (Fig. S5 H; Kurachi et al., 2014). We further overlapped their cobinding genes with BATF- or IRF4-regulated genes identified from their RNA-seq data respectively, and found that STAT3 occupied numerous genes directly regulated by BATF or IRF4 (Fig. 7 G and Table S6). For example, STAT3, BATF, and IRF4 all occupied the promoter of *Gzmb* gene, and both the chromatin accessibility and H3K27ac modification were reduced at this locus in *Stat3*$^{-/-}$ CD8$^+$ T cells (Fig. 7 H). In addition, these three transcription factors were shown to cobind to the intron and promoter regions of *Havcr2* gene and the distal enhancer of *Tbx21* gene, and *Stat3* deficiency declined the accessibilities and H3K27ac modifications at these gene loci

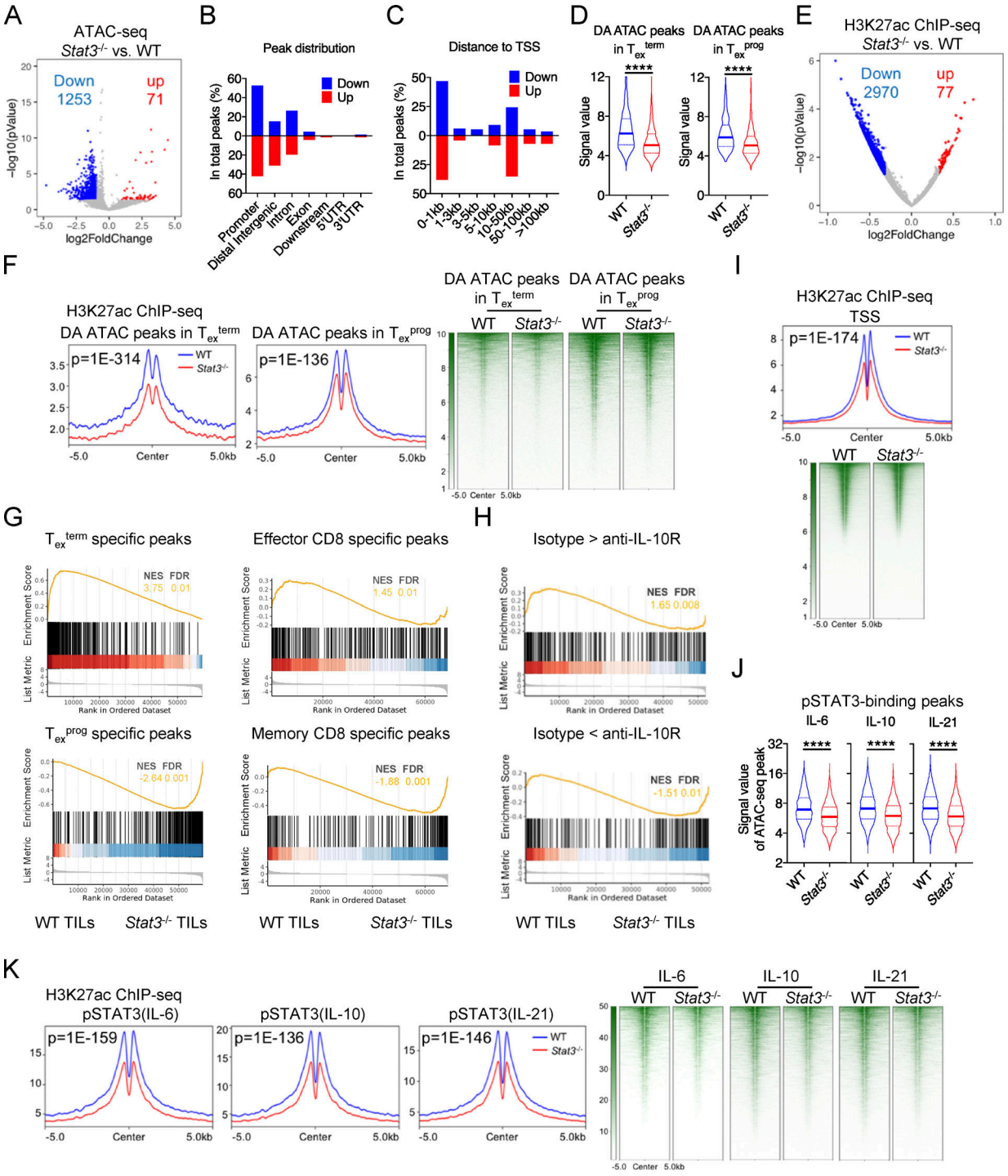

Figure 6. **STAT3 regulates the epigenetic landscape of T_{ex} cells in cancer. (A)** Volcanic plot showing OCR peak changes between WT and *Stat3*$^{-/-}$ OT-I TILs. **(B)** Genetic feature distribution of changed OCR peaks between WT and *Stat3*$^{-/-}$ OT-I TILs. **(C)** Distribution relative to TSS of changed OCR peaks between WT and *Stat3*$^{-/-}$ OT-I TILs. **(D)** Violin plots showing the signal values of OCR peaks in WT and *Stat3*$^{-/-}$ OT-I TILs at T_{ex}^{term} or T_{ex}^{prog} DA peaks (GEO accession no. GSE123236). **(E)** Volcanic plot showing differentially H3K27ac modified regions (DMRs) between IL-10–stimulated WT and *Stat3*$^{-/-}$ CD8$^+$ T cells. DMRs were filtered by fold change >1.25 and P value <0.05. **(F)** Peak plots (left panel) and heatmaps (right panel) showing the deposition of H3K27ac modification centered on T_{ex}^{term} or T_{ex}^{prog} DA peaks in WT and *Stat3*$^{-/-}$ OT-I TILs (GEO accession no. GSE123236). P value by Fisher test was added in the plot. **(G and H)** PSEA results for comparing the enrichment of signature OCR peaks in other CD8$^+$ T cell subsets in WT and *Stat3*$^{-/-}$ OT-I TILs (GEO accession nos. GSE123236, GSE86797, and GSE116389). NES, normalized enrichment score; FDR, false discovery rate q-value. **(I)** Peak plot (upper panel) and heatmap (bottom panel) showing the deposition of H3K27ac modification centered on TSS in WT and *Stat3*$^{-/-}$ OT-I TILs. P value by Fisher test was added in the plot. **(J)** Violin plots showing the signal values of OCR peaks in WT and *Stat3*$^{-/-}$ OT-I TILs at pSTAT3-binging sites. **(K)** Peak plots (left panel) and heatmaps (right panel) showing the deposition of H3K27ac modification centered on pSTAT3-binding peaks in WT and *Stat3*$^{-/-}$ OT-I TILs. P value by Fisher test was added in the plot. *, P < 0.05; **, P < 0.01; ***, P < 0.001; ****, P < 0.0001 by unpaired two-tailed Student's *t* test (D and J).

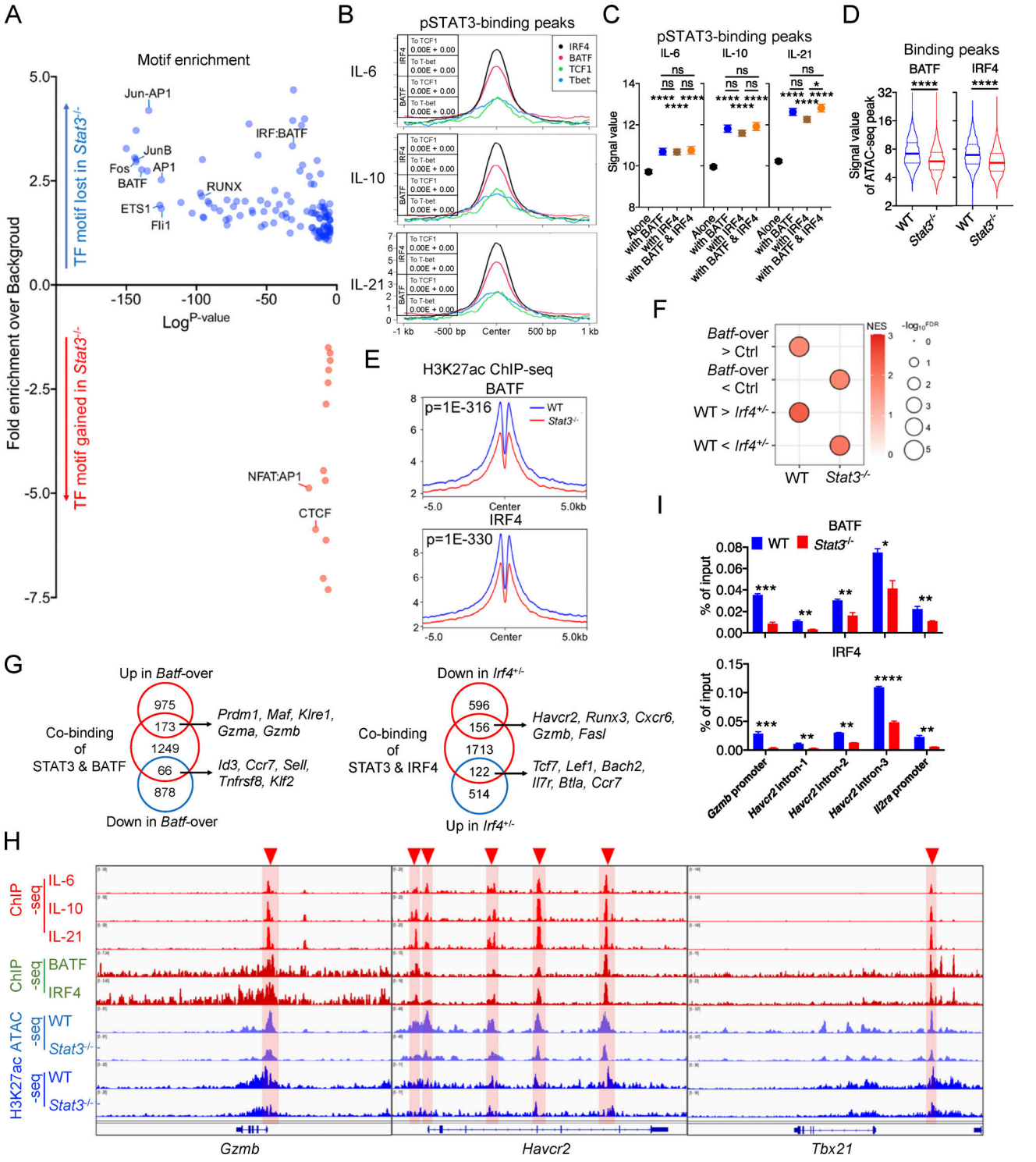

Figure 7. **STAT3 cooperates with BATF and IRF4 to mediate T_{ex}^{term} cell development. (A)** Enrichment of known transcription factor–binding motifs in DA OCR peaks between WT and *Stat3*$^{-/-}$ OT-I TILs. The x and y axes represent the $\log^{P\ value}$ and fold change of motif enrichment separately. Targeted motifs were compared to the whole genome background to calculate the P value and fold change. **(B)** Peak plots for read density profiles of BATF, IRF4, TCF1, and T-bet occupations centered on pSTAT3-binding peaks in CD8$^+$ T cells (GEO accession nos. GSE54191, GSM5016615, and GSE96724). Values were normalized to the total number of reads. P value by Chi-squared test was added in the plot. **(C)** Signal values of pSTAT3-binding peaks in IL-6–, IL-10–, and IL-21–stimulated CD8$^+$ T cells at BATF- or IRF4-binding sites or not. **(D)** Violin plots showing the signal values of OCR peaks in WT and *Stat3*$^{-/-}$ OT-I TILs at BATF- or IRF4-binging sites. **(E)** Peak plots showing the deposition of H3K27ac modification centered on BATF- or IRF4-binging sites in WT and *Stat3*$^{-/-}$ OT-I TILs. P value by Fisher test was added in the plot. **(F)** GSEA results for comparing the enrichment of BATF- and IRF4-regulated feature genes in the transcriptomes of WT and *Stat3*$^{-/-}$ OT-I TILs (GEO accession nos. GSE154745 and GSE84820). NES, normalized enrichment score; FDR, false discovery rate q-value. FDR presented as $-\log_{10}^{(FDR)}$. **(G)** Venn diagrams of pSTAT3 and BATF-cobinding genes and BATF-regulated genes (left panel), or of pSTAT3 and IRF4-cobinding genes and IRF4-regulated genes (right panel) in CD8$^+$ T cells. **(H)** Aligned ChIP-seq tracks of pSTAT3, BATF, and IRF4 in CD8$^+$ T cells, ATAC-seq tracks of WT and *Stat3*$^{-/-}$ OT-I TILs, and

H3K27ac ChIP-seq tracks of WT and *Stat3*$^{-/-}$ CD8$^+$ T cells at the specific gene loci. **(I)** ChIP assays were performed with in vitro IL-10–stimulated WT and *Stat3*$^{-/-}$ CD8$^+$ T cells with anti-BATF or anti-IRF4. The relative amount of immune-precipitated DNA was detected by real-time PCR and normalized relative to the input control. Data are representative of two (I) independent experiments. Data are shown as mean ± SEM. *, P < 0.05; **, P < 0.01; ***, P < 0.001; ****, P < 0.0001 by unpaired two-tailed Student's *t* test (C, D, and I).

(Fig. 7 H). Similar occupancies and epigenetic changes were also found in *Prdm1*, *Il2ra*, and *Prf1* gene loci as shown (Fig. S5 I).

It was previously reported that STAT3-binding efficiency was greatly diminished in *Irf4*-deficient CD4$^+$ T cells (Kwon et al., 2009). To further investigate whether STAT3 had any effect on the occupation of BATF and IRF4 around the genome, we determined the binding of BATF and IRF4 to their target genes in *Stat3*$^{-/-}$ CD8$^+$ T cells. ChIP-qPCR results showed that the binding of BATF and IRF4 to the loci of *Gzmb*, *Havcr2*, and *Il2ra* genes was significantly reduced in IL-10–stimulated *Stat3*$^{-/-}$ as compared with IL-10–stimulated WT CD8$^+$ T cells (Fig. 7 I). Thus, these results altogether indicate that STAT3 might function cooperatively with BATF and IRF4 in regulating T_{ex}^{term} cell development and function.

Discussion

The molecular mechanisms whereby the extrinsic factors regulate CD8$^+$ T cell differentiation and function, especially in cancer, are still not well understood. In this study, we found that *Stat3* deficiency in CD8$^+$ T cells impaired their effector functions and worsened tumor controls. IL-10 and IL-21 activate STAT3 signaling to promote T_{ex}^{term} cell development and survival and enhance their effector functions in cancer. Moreover, STAT3 also plays a similar role in promoting terminally differentiated effector CD8$^+$ T cell development and function in acute infection. Mechanistically, STAT3 directly promotes the expression of T_{ex}^{term}-related genes, while it suppressed those of the T_{ex}^{prog} cells. Moreover, STAT3 also regulates the chromatin accessibility for T_{ex}^{term} fate commitment, in collaboration with BATF and IRF4.

STAT3 is a polyfunctional transcription factor that can be activated by various extrinsic and intracellular molecules (Kane et al., 2014). During CD8$^+$ T cell priming and exhaustion, multiple cytokines are involved in STAT3 activation (Guo et al., 2021; Xin et al., 2015). IL-6 specifically induces STAT3 activation in naive CD8$^+$ T cells and has a role in CD8$^+$ T cell activation (Bottcher et al., 2014), but with limited functions in T_{ex} cells within tumors. In contrast, IL-10 specifically functions in the process of T cell exhaustion but not early activation in tumor models, and the IL-21–STAT3 axis acts on CD8$^+$ T cells during both activation and exhaustion. Moreover, both IL-10 and IL-21 are previously shown to be enriched in the tumor microenvironment, mainly derived from CD4$^+$ T cells (Cui et al., 2021; Sawant et al., 2019; Snell et al., 2018; Zander et al., 2019). Besides IL-10 and IL-21, there may exist other mediators inducing STAT3 phosphorylation in T_{ex} cells within tumors, which needs to be further investigated (Yu et al., 2014). For example, IL-27, a member of the IL-6/IL-12 family regulating CD8$^+$ T cell exhaustion in chronic infection and cancer, is shown to induce STAT3, besides STAT1, activation in T cells (Chihara et al., 2018; Hirahara et al., 2015; Huang et al., 2019; Owaki et al., 2008). In addition, some microRNAs and even hypoxia may also induce STAT3 activation in immune cells within tumors (Gao et al., 2017; Yu et al., 2014). Moreover, besides canonical homodimer, STAT3 can also interact with STAT1, STAT4, or STAT5 and form heterodimers in response to cytokines and CSF signaling (Delgoffe and Vignali, 2013), which implies the other potential mechanisms of STAT3 activation and function.

IL-10 and IL-21 functions, though have been reported in previous studies (Cui et al., 2011; Elsaesser et al., 2009; Fröhlich et al., 2009; Guo et al., 2021; Hanna et al., 2021; Ren et al., 2020; Xin et al., 2015; Yi et al., 2009; Zander et al., 2022), still remain controversial and lack mechanistic analysis. Briefly, IL-10 is shown to promote memory CD8$^+$ T cell development in acute LCMV infection and the leukemia model (Cui et al., 2011; Hanna et al., 2021), but is also reported to enhance TIM-3$^+$ CD8$^+$ T cell development and expansion in B16 melanoma models (Guo et al., 2021; Sawant et al., 2019). IL-21 is shown not only to be critical in memory CD8$^+$ T cell maturation in acute LCMV infection (Cui et al., 2011) but also functions to enhance CX3CR1$^+$ or Granzyme B$^+$ effector CD8$^+$ T cell development in chronic LCMV infection and tumor models (Cui et al., 2021; Snell et al., 2018; Zander et al., 2022; Zander et al., 2019). Here, we systematically determined the functions of IL-10 and IL-21 in STAT3 signaling by phenotypical and transcriptional analyses. Both IL-10 and IL-21 had critical roles in promoting T_{ex}^{term} cell development, at least partially, in a STAT3-dependent manner. In addition, IL-10 and IL-21 also exert potent functions in promoting cytotoxicity, protecting against apoptosis, and enhancing the fitness of CD8$^+$ T cells via STAT3 signaling. In addition to T_{ex}^{term} cells, STAT3 signaling also plays an important role in T_{ex}^{prog} cells in cancer, although it is not absolutely required for their development. Considering the importance of T_{ex}^{prog} cells in the long-term persistence of antitumor immunity and their ability to develop into T_{ex}^{term} cells (Miller et al., 2019), it is possible that in the absence of STAT3, T_{ex}^{term} cells were defective, at least in part, secondary to impaired T_{ex}^{prog} cells, especially at a later stage.

In acute infection, CD8$^+$ T cells differentiate into TCF1$^+$ memory precursors and Granzyme B–producing terminally differentiated CD8$^+$ T cells, similar to tumor-specific T_{ex}^{prog} and T_{ex}^{term} cells, respectively, in their transcriptomes and functions to some extent. However, there are differences in the microenvironment between cancer and acute infection, resulting in many differences between tumor-specific T_{ex} cells and effector or memory CD8$^+$ T cells (McLane et al., 2019). One major difference is the increased and sustained expression of inhibitory receptors, including PD-1, TIM-3, TIGIT, 2B4, and LAG3, which are induced by chronic TCR stimulation (McLane et al., 2019). Terminally differentiated CD8$^+$ T cells arise from TCF-1$^+$ stem-like T cells in tumor microenvironments, in which STAT3 plays

critical roles. Its role in the differentiation of effector T cells in acute infection requires further investigation.

There are two functional phosphorylated sites in the STAT3 protein located at Tyr705 and Ser727 residues (You et al., 2015). Phosphorylation of Tyr705 residue dominantly leads to the dimerization and nuclear translocation of STAT3 protein for the binding and transcriptional regulation of target genes (You et al., 2015). Phosphorylation at Ser727 residue mainly mediates mitochondrial localization and favors mitochondrial functions and OXPHOS (Huynh et al., 2019; Wegrzyn et al., 2009; You et al., 2015). pS727 can also facilitate transcriptional regulation by STAT3 (Wen et al., 1995). In this study, both Tyr705 and Ser727 residues are deleted in mature CD8$^+$ T cells in *Stat3*$^{fl/fl}$*Cd8a*^{Cre} mice (Takeda et al., 1998). By performing ChIP-seq for STAT3(pY705)-binding sites in the whole genome, we demonstrated that pSTAT3 directly bound to the loci of numerous T_{ex}^{term}-related genes (e.g., *Id2*, *Prdm1*, and *Havcr2*) and transcriptionally promoted their expression for T_{ex}^{term} cell development in cancer. Moreover, pSTAT3 also directly regulated the expression of *Gzmb* and *Prf1* via binding to their promoters, thereby enhancing cytotoxic responses. In addition, STAT3 was also shown to be critical in promoting OXPHOS of T_{ex} cells within tumors in this study. It is previously demonstrated that promoting OXPHOS in T_{ex}^{term} cells dramatically enhances their expansion and cytotoxicity (Guo et al., 2021). Thus, it is possible that besides transcriptional regulation, STAT3 may also function via S727 phosphorylation to further promote T_{ex}^{term} cell fitness and function, which needs to be further investigated.

The cooperation of STAT3 with AP-1 transcription factors (e.g., BATF and IRF4) has been reported in B cells and CD4$^+$ T cells (Ciofani et al., 2012; Kwon et al., 2009; Xu et al., 2019). It is demonstrated that IRF4 cooperates with STAT3 to regulate IL-21–dependent gene expression in B cells (Kwon et al., 2009; Li and Leonard, 2018) and the IL-21–STAT3–BATF axis is required for sustaining the effector function of CD8$^+$ T cells in chronic infections (Xin et al., 2015). Here, we analyzed the functional relationships between STAT3 and BATF/IRF4 in T_{ex} cell differentiation by multiomics approaches. STAT3 had extensive co-occupancy in T_{ex} fate-related gene loci with BATF and IRF4 across the whole genome in CD8$^+$ T cells. Moreover, it epigenetically promoted chromatin accessibility for the efficient binding of BATF and IRF4 to target loci in activated CD8$^+$ T cells. Hence, these data revealed a complex regulatory network involving STAT3 and AP-1 factors (e.g., BATF and IRF4) in the fate determination of CD8$^+$ T cells during exhaustion.

Harnessing STAT3 signaling in improving cancer immunotherapies has been attempted a few times. For example, it is shown that fusing a STAT3-binding motif from IL-21 receptor into CD19 CAR against acute B lymphoblastic leukemia, with the goal of activating STAT3 signaling, results in superior antitumor effects (Kagoya et al., 2018). Recombinant human IL-6/IL-6Rα fusion protein and constitutively active GP130 or p40 subunit from IL-23/IL-12 both improve CAR-T cells in antitumor efficacy against B cell leukemia and solid tumors (Jiang et al., 2020; Ma et al., 2020). Moreover, it is reported that IL-21–primed polyclonal antigen–specific CD8$^+$ T cells combined with CTLA-4 blockade induces long-term remission in a melanoma patient (Chapuis et al., 2016), and human CAR-modified CD8$^+$ T cells treated with affinity-enhanced IL-10 variants, with greater STAT3 activation, display robust antitumor activities in vitro against leukemic cells (Gorby et al., 2020). Therefore, our research has provided a mechanistic basis for a STAT3-enhancing strategy in cancer immunotherapies and may benefit the further development of novel T cell– and cytokine-based therapies in the future.

Materials and methods

Mice

C57BL/6, CD45.1, *Tcrbd*$^{-/-}$, and OT-I (TCR specific for E.G7 and B16-OVA $K^bOVA_{257-264}$) congenic mice were maintained in-house. *Stat3*$^{fl/fl}$ (Takeda et al., 1998) and *Il6ra*$^{fl/fl}$ mice (McFarland-Mancini et al., 2010) were crossed with *Cd8a*^{Cre} mice (Maekawa et al., 2008) and then were bred with OT-I mice. Rosa26-Cas9 mice were bred with OT-I mice. All animal experiments conducted at Tsinghua University were approved by the Institutional Animal Care and Use Committee. 6–8-wk-old, male and female, age and sex-matched mice were used for all experiments.

Listeria monocytogenes (LM) infection

Erythromycin-resistant LM expressing $OVA_{257-264}$ (LM-OVA) were grown in brain heart infusion media supplemented with 5 µg/ml erythromycin. 1 × 10^5 CFU of LM-OVA were resuspended in 100 µl PBS and injected intravenously (i.v.) into 6–8-wk-old mice. The infected mice were analyzed on day 8 after injection.

Tumor inoculation

B16-OVA cells were cultured in a DMEM medium with 10% FBS, penicillin, and streptomycin. E.G7 (EL4-OVA) cells were cultured in RPMI 1640 medium with 10% FBS, penicillin, and streptomycin. 1 × 10^6 E.G7 or 2 × 10^5 B16-OVA cells were resuspended in 100 µl PBS and injected subcutaneously (s.c.) into 6- to 8-wk-old mice. Tumor growth was monitored every 2 or 3 d. Tumor volume was calculated by the following formula: tumor volume = π × length × width^2/6.

Isolation of TILs

E.G7 and B16-OVA tumors were digested with 1 mg/ml collagenase D supplemented with 10 U/ml DNase I for 40 min at 37°C prior to centrifugation on a discontinuous Percoll gradient (GE Healthcare).

Flow cytometry

Single cells were suspended in PBS and incubated with antibodies against surface molecules for 30 min at 4°C. Dead cells were excluded based on viability dye staining (Fixable viability dye eF506; eBioscience). For intracellular cytokine detection, cells were stimulated with PMA (50 ng/ml; Sigma-Aldrich) and ionomycin (500 ng/ml; Sigma-Aldrich) in the presence of Brefeldin A (Golgiplug, BD Bioscience) for 5 h prior to staining. For intracellular staining, surface-stained cells were fixed and permeabilized with the Foxp3/Transcription Factor Staining Buffer

Set (eBiosciences), followed by incubation with fluorochrome-conjugated antibodies.

For the detection of phosphorylated STAT3, cells were cultured in a fresh medium supplied with cytokines for 30 min, resuspended in cold PBS, and stained with antibodies against surface molecules. Then the cells were fixed with Phosflow Lyse/Fix buffer (BD Bioscience), followed by 90% methanol permeabilization and staining with antibodies against phosphorylated STAT3 in PBS. For analysis, the cells were acquired on an LSRFortessa (BD) flow cytometer, and data were analyzed using FlowJo 10.4.

Naive CD8$^+$ T cell adoptive transfer

CD8$^+$ T cells were purified from spleens and lymph nodes using Dynabeads FlowComp Mouse CD8 Kit (Invitrogen). Naive CD8$^+$CD25$^-$CD44^{low}CD62L^{hi} T cells were FACS-sorted from purified CD8$^+$ T cells on a FACS Aria (BD) flow cytometer. The purity of the sorted cells was >99%. Then 0.3 million FACS-sorted naive CD45.1/2 WT and CD45.2 *Stat3*$^{-/-}$ OT-I cells were mixed at a 1:1 ratio and transferred (i.v.) into CD45.1 recipients 1 d prior to B16-OVA tumor inoculation.

In vitro activation and stimulation

FACS-sorted naive CD8$^+$ T cells were activated with the plate-bound anti-CD3 (clone 145-2C11, 5 µg/ml; BioXCell) and anti-CD28 (clone 37.51, 1 µg/ml; BioXCell) for 3 d. Then activated CD8$^+$ T cells were cultured at 37°C for another 3 d in fresh medium with 10 ng/ml IL-6, 10 ng/ml IL-10, or 10 ng/ml IL-21.

Il10ra knockout

Single-guide RNA targeting *Il10ra* were designed on the CHOP-CHOP website as sg-*Il10ra*-1 (5′- TGATCTCACAACGTTCACCC-3′) and sg-*Il10ra*-2 (5′-GATCTGTATCACCGAAGCTA-3′). Single-guide RNA was cloned into pWKO retroviral expression vectors which also encoded IRES-BFP cassettes. Empty vectors were used as controls. Retrovirus plasmids and pCL-ECO (packaging plasmid) were transfected into the Phoenix cell line using calcium phosphate. Retrovirus supernatant was harvested 48 h after transfection. FACS-sorted naive CD8$^+$ T cells were activated with the plate-bound anti-CD3 (5 µg/ml) and anti-CD28 (5 µg/ml) for 48 h. Activated CD8$^+$ T cells were infected with retrovirus in the presence of polybrene (1 µg/ml) with spin (1,800 rpm, 32°C) for 90 min, and medium was replaced 4 h after infection.

In vitro killing assay

Naive WT and *Stat3*$^{-/-}$ OT-I cells were activated in vitro for 3 d and then stimulated with IL-10 for another 3 d. B16-OVA tumor cells were labeled with CFSE at 37°C for 5 min, mixed with CD8$^+$ T cells at 1:10, 1:4, 1:2, 1:1, and 2:1 ratios, and incubated at 37°C for 5 h. Intracellular cleaved caspase 3-PE in CFSE$^+$ B16-OVA tumor cells were measured by flow cytometry.

In vitro proliferation assay

Naive WT and *Stat3*$^{-/-}$ CD8$^+$ T cells were mixed and activated in vitro for 3 d and then labeled with CTV at 37°C for 5 min. CTV-labeled CD8$^+$ T cells were stimulated by IL-6, IL-10, or IL-21 in anti-CD3/anti-CD28–bound plate. 2 or 3 d later, CTV in CD8$^+$ T cells was measured by flow cytometry.

RNA processing and real-time quantitative PCR (RT-qPCR) analysis

Total cellular RNA was extracted from CD8$^+$ T cells with Magzol reagent (Magen). M-MLV reverse transcription kit (Invitrogen) was used for generating cDNA. Gene expression at the mRNA level was measured using the SYBR real-time kit (Bio-Rad Laboratories). For RT-qPCR analysis, the data shown were normalized to the expression of the reference gene *Actb*. The following genes were amplified with primers as described: *Actb*, 5′-TGGAATCCTGTGGCATCCATGAAAC-3′ and 5′-TAAAACGCAGCTCAGTAACAGTCCG-3′; *Id3*, 5′- CTGTCGGAACGTAGCCTGG-3′ and 5′-GTGGTTCATGTCGTCCAAGAG-3′; *Ccr7*, 5′-CTTTCTTGTATGCCTTCATC-3′ and 5′- GGTTAAGCAGTTTCTTAGGT-3′; *Id2*, 5′-ATGAAAGCCTTCAGTCCGGTG-3′ and 5′-AGCAGACTCATCGGGTCGT-3′; and *Gzmb*, 5′-CCACTCTCGACCCTACATGG-3′ and 5′-GGCCCCCAAAGTGACATTTATT-3′.

RNA-seq and ATAC-seq

Cotransferred WT and *Stat3*$^{-/-}$ OT-I cells were FACS-sorted from B16-OVA tumors at about day 16 after inoculation for RNA-seq and ATAC-seq. For RNA-seq, total RNA was extracted and sent to BGI Genomics for library construction. The library products were sequenced via Illumina Hiseq4000 by BGI Genomics. Low-quality reads and adaptor sequences were removed by Trim Galore v0.4.4. The clean reads were aligned to mm10 by bowtie2 with default parameter (Langmead and Salzberg, 2012), and uniquely mapping reads were summarized by featureCounts (from Subread package). Differentially expressed genes (DEGs) were identified by at least twofold change and a false discovery rate (FDR) adjusted P value of 0.05 by using DESeq2. ClusterProfiler (R package) was used for pathway analysis (Yu et al., 2013).

For ATAC-seq, FACS-sorted OT-I TILs were processed and analyzed as indicated (Chang et al., 2020). PSEA was performed as indicated (Khan et al., 2019).

ChIP-seq and ChIP-qPCR

FACS-sorted naive CD8$^+$ T cells were activated with the plate-bound anti-CD3 (5 µg/ml) and anti-CD28 (1 µg/ml) for 3 d. For pSTAT3 ChIP-seq, the activated WT CD8$^+$ T cells were cultured at 37°C for 30 min in fresh medium with 10 ng/ml IL-6, 10 ng/ml IL-10, or 10 ng/ml IL-21. For H3K27ac ChIP-seq, the activated WT and *Stat3*$^{-/-}$ CD8$^+$ T cells were stimulated by 10 ng/ml IL-10 for another 3 d. For BATF and IRF4 Chip experiment, the activated WT and *Stat3*$^{-/-}$ CD8$^+$ T cells were stimulated by 10 ng/ml IL-10 for another 3 d. Then CD8$^+$ T cells were fixed by 1% paraformaldehyde, followed by digestion and sonication. Chromatin from 1 × 10^7 lived cells was used for each ChIP experiment. 7.5 µg anti-pSTAT3(Y705) antibody, 1 µg anti-H3K27ac antibody, 7.5 µg anti-BATF antibody, or 7.5 µg anti-IRF4 antibody was used.

The ChIP experiment was performed as indicated (Xu et al., 2019). Sequencing reads were mapped to the mouse genome mm10 by bowtie2 (Langmead and Salzberg, 2012). PCR duplicates were removed using Picard MarkDuplicates. The uniquely

mapped reads were used to call peak with MACS2 using a P value cutoff of 0.01 (Zhang et al., 2008). ChIPseeker was used for peak annotation (Yu et al., 2015). Overlapped peaks were identified by bedtools intersect. Deeptools was used for comparing profiles of different ChIPseq samples (including those from Gene Expression Omnibus [GEO] datasets; Ramirez et al., 2016). HOMER was used for motif discovery.

The enriched heatmaps of pSTAT3 ChIP-seq signal profiles were generated with Deeptools (V3.5.0; Ramirez et al., 2016). The computeMatrix was used to calculate scores for the top 3,000 peak sites of pSTAT3 with the following parameters: reference-point--referencePoint center. The plotHeatmap was used to create the heatmap for scores associated with the genomic regions with the following parameters: --zMin 1 --zMax 10 --kmeans 1.

For ChIP-qPCR analysis, the following DNA fragments were amplified with primers as described: *Gzmb* promoter, 5′-TAC CATAGGCTACAAACCCCACCC-3′ and 5′-CGTCAAGAGTGTTGT CCTTGCTC-3′; *Havcr2* intron-1, 5′-TGAGTGCAACCTGGGTTGC-3′ and 5′-TTCACCACATGCAATCTCTAAAGTG-3′; *Havcr2* intron-2, 5′-AACTTTTGTGTGTATGGCTGC-3′ and 5′-GTAAGAGGCCAA CATGGTCAG-3′; *Havcr2* intron-3, 5′-GAGGACAGCCTCTTGTTC TAGTC-3′ and 5′-GTTAGGAGAGCACATTCAGACATG-3′; and *Il2ra* promoter, 5′-TGACAGACTGAGAGGCCTGA-3′ and 5′-TGG GTCAACCCCTTTACTGC-3′.

scRNA-seq analysis

Gene expression information was downloaded from the website for public human scRNA-seq database (Lung, http://lung.cancer-pku.cn; HCC, http://hcc.cancer-pku.cn/; and CRC, http://crc.cancer-pku.cn/; Guo et al., 2018; Zhang et al., 2018; Zheng et al., 2017). The expression unit was normalized expression/log(TPM+1). PD-1^{hi} cells were filtered using an expression value cutoff of 5.00.

Statistical analysis

Statistical analysis was performed with Graph Prism 8.2.0 (GraphPad software) and presented as mean ± SEM unless specifically indicated. For two group comparisons, statistical analysis was performed with unpaired or paired two-tailed Student's *t* tests. For multiple group comparisons, statistical analysis was performed with one-way ANOVA followed by Tukey's multiple comparisons test. Tumor growth data were compared by two-way ANOVA followed by Tukey's multiple comparisons test. P values <0.05 were considered statistically significant (*, P < 0.05; **, P < 0.01; ***, P < 0.001; ****, P < 0.0001). Statistical details for each experiment can be found in the figures and the legends.

Online supplemental material

Fig. S1 shows data further supporting the results in Fig. 1. Fig. S2 shows data further supporting the results in Fig. 2. Fig. S3 shows data further supporting the results in Fig. 4. Fig. S4 shows data further supporting the results in Fig. 5. Fig. S5 shows data further supporting the results in Fig. 7. Table S1 lists the DEGs in WT vs. *Stat3*$^{-/-}$ OT-I cells from B16-OVA tumors. Table S2 lists STAT3-binding and -regulated genes. Table S3 lists STAT3-induced or -suppressed feature genes. Table S4 lists DA peaks in WT vs. *Stat3*$^{-/-}$ OT-I cells from B16-OVA tumors. Table S5 lists differentially H3K27ac modified regions (DMRs) between IL-10–stimulated WT and *Stat3*$^{-/-}$ CD8^{+} T cells. Table S6 lists STAT3- and BATF/IRF4-coregulated genes.

Data availability

Data from RNA-seq of WT vs. *Stat3*$^{-/-}$ OT-I cells transferred into B16-OVA–bearing mice (Fig. 2) are available in the GEO database under accession no. GSE217375. Data from ATAC-seq of WT vs. *Stat3*$^{-/-}$ OT-I cells transferred into B16-OVA–bearing mice (Fig. 6) are available in the GEO database under accession no. GSE217372. ChIP-seq of pSTAT3 in CD8^{+} T cells (Fig. 5) and ChIP-seq of H3K27ac in WT vs. *Stat3*$^{-/-}$ CD8^{+} T cells (Fig. 6) are available in the GEO database under accession no. GSE217374.

Acknowledgments

We thank Dr. Wenwen Zeng (Institute for Immunology, Tsinghua University, Beijing, China) for providing *Il6ra*$^{fl/fl}$ mice.

This work was supported by grants from the Natural Science Foundation of China (31991173, 31821003, and 31991170), the National Key Research and Development Program of China (2021YFC2302403), Tsinghua University Spring Breeze Fund (2020Z99CFG008), Innovative Research Team of High-level Local Universities in Shanghai, Tsinghua University-Xiamen Chang Gung Hospital Joint Research Center for Anaphylactic Disease, and Shanghai Jiao Tong University-Bennu Biotherapeutics Joint Laboratory for Cell Therapy.

Author contributions: Q. Sun and C. Dong designed the project and analyzed the data. Q. Sun conducted the experiments. D. Liu, B. Pan, X. Chi, P. Wei, D. Cai. W. Xu, K. Wei, Z. Zhao, and Y. Fu helped with the experiments. X. Zhao and R. Li analyzed the bioinformatics data. Q. Sun, C. Dong, L. Ni, and B. Xie prepared the manuscript.

Disclosures: The authors declare no competing interests exist.

Submitted: 20 April 2022
Revised: 5 November 2022
Accepted: 4 January 2023

References

Angelosanto, J.M., S.D. Blackburn, A. Crawford, and E.J. Wherry. 2012. Progressive loss of memory T cell potential and commitment to exhaustion during chronic viral infection. *J. Virol.* 86:8161–8170. https://doi.org/10.1128/JVI.00889-12

Böttcher, J.P., O. Schanz, C. Garbers, A. Zaremba, S. Hegenbarth, C. Kurts, M. Beyer, J.L. Schultze, W. Kastenmüller, S. Rose-John, and P.A. Knolle. 2014. IL-6 trans-signaling-dependent rapid development of cytotoxic CD8^{+} T cell function. *Cell Rep.* 8:1318–1327. https://doi.org/10.1016/j.celrep.2014.07.008

Callahan, M.K., M.A. Postow, and J.D. Wolchok. 2016. Targeting T cell Co-receptors for cancer Therapy. *Immunity*. 44:1069–1078. https://doi.org/10.1016/j.immuni.2016.04.023

Chang, D., Q. Xing, Y. Su, X. Zhao, W. Xu, X. Wang, and C. Dong. 2020. The conserved non-coding sequences CNS6 and CNS9 control cytokine-induced rorc transcription during T helper 17 cell differentiation. *Immunity*. 53:614–626.e4. https://doi.org/10.1016/j.immuni.2020.07.012

Chapuis, A.G., S.M. Lee, J.A. Thompson, I.M. Roberts, K.A. Margolin, S. Bhatia, H.L. Sloan, I. Lai, F. Wagener, K. Shibuya, et al. 2016. Combined IL-21-primed polyclonal CTL plus CTLA4 blockade controls refractory metastatic melanoma in a patient. *J. Exp. Med.* 213:1133–1139. https://doi.org/10.1084/jem.20152021

Chen, J., I.F. López-Moyado, H. Seo, C.J. Lio, L.J. Hempleman, T. Sekiya, A. Yoshimura, J.P. Scott-Browne, and A. Rao. 2019. NR4A transcription factors limit CAR T cell function in solid tumours. *Nature*. 567:530–534. https://doi.org/10.1038/s41586-019-0985-x

Chen, Y., R.A. Zander, X. Wu, D.M. Schauder, M.Y. Kasmani, J. Shen, S. Zheng, R. Burns, E.J. Taparowsky, and W. Cui. 2021. BATF regulates progenitor to cytolytic effector CD8$^+$ T cell transition during chronic viral infection. *Nat. Immunol.* 22:996–1007. https://doi.org/10.1038/s41590-021-00965-7

Chihara, N., A. Madi, T. Kondo, H. Zhang, N. Acharya, M. Singer, J. Nyman, N.D. Marjanovic, M.S. Kowalczyk, C. Wang, et al. 2018. Induction and transcriptional regulation of the co-inhibitory gene module in T cells. *Nature*. 558:454–459. https://doi.org/10.1038/s41586-018-0206-z

Ciofani, M., A. Madar, C. Galan, M. Sellars, K. Mace, F. Pauli, A. Agarwal, W. Huang, C.N. Parkhurst, M. Muratet, et al. 2012. A validated regulatory network for Th17 cell specification. *Cell*. 151:289–303. https://doi.org/10.1016/j.cell.2012.09.016

Cui, C., J. Wang, E. Fagerberg, P.M. Chen, K.A. Connolly, M. Damo, J.F. Cheung, T. Mao, A.S. Askari, S. Chen, et al. 2021. Neoantigen-driven B cell and CD_4 T follicular helper cell collaboration promotes anti-tumor CD8 T cell responses. *Cell*. 184:6101–6118.e13. https://doi.org/10.1016/j.cell.2021.11.007

Cui, W., Y. Liu, J.S. Weinstein, J. Craft, and S.M. Kaech. 2011. An interleukin-21-interleukin-10-STAT3 pathway is critical for functional maturation of memory CD8$^+$ T cells. *Immunity*. 35:792–805. https://doi.org/10.1016/j.immuni.2011.09.017

Delgoffe, G.M., and D.A. Vignali. 2013. STAT heterodimers in immunity: A mixed message or a unique signal? *JAKSTAT*. 2:e23060. https://doi.org/10.4161/jkst.23060

Dong, C. 2021. Cytokine regulation and function in T cells. *Annu. Rev. Immunol.* 39:51–76. https://doi.org/10.1146/annurev-immunol-061020-053702

Darnell, J.E.Jr. 1997. STATs and gene regulation. *Science*. 277:1630–1635. https://doi.org/10.1126/science.277.5332.1630

Elsaesser, H., K. Sauer, and D.G. Brooks. 2009. IL-21 is required to control chronic viral infection. *Science*. 324:1569–1572. https://doi.org/10.1126/science.1174182

Emmerich, J., J.B. Mumm, I.H. Chan, D. LaFace, H. Truong, T. McClanahan, D.M. Gorman, and M. Oft. 2012. IL-10 directly activates and expands tumor-resident CD8(+) T cells without de novo infiltration from secondary lymphoid organs. *Cancer Res.* 72:3570–3581. https://doi.org/10.1158/0008-5472.CAN-12-0721

Fröhlich, A., J. Kisielow, I. Schmitz, S. Freigang, A.T. Shamshiev, J. Weber, B.J. Marsland, A. Oxenius, and M. Kopf. 2009. IL-21R on T cells is critical for sustained functionality and control of chronic viral infection. *Science*. 324:1576–1580. https://doi.org/10.1126/science.1172815

Gao, P., N. Niu, T. Wei, H. Tozawa, X. Chen, C. Zhang, J. Zhang, Y. Wada, C.M. Kapron, and J. Liu. 2017. The roles of signal transducer and activator of transcription factor 3 in tumor angiogenesis. *Oncotarget*. 8:69139–69161. https://doi.org/10.18632/oncotarget.19932

Gorby, C., J. Sotolongo Bellón, S. Wilmes, W. Warda, E. Pohler, P.K. Fyfe, A. Cozzani, C. Ferrand, M.R. Walter, S. Mitra, et al. 2020. Engineered IL-10 variants elicit potent immunomodulatory effects at low ligand doses. *Sci. Signal.* 13:eabc0653. https://doi.org/10.1126/scisignal.abc0653

Guo, X., Y. Zhang, L. Zheng, C. Zheng, J. Song, Q. Zhang, B. Kang, Z. Liu, L. Jin, R. Xing, et al. 2018. Global characterization of T cells in non-small-cell lung cancer by single-cell sequencing. *Nat. Med.* 24:978–985. https://doi.org/10.1038/s41591-018-0045-3

Guo, Y., Y.Q. Xie, M. Gao, Y. Zhao, F. Franco, M. Wenes, I. Siddiqui, A. Bevilacqua, H. Wang, H. Yang, et al. 2021. Metabolic reprogramming of terminally exhausted CD8$^+$ T cells by IL-10 enhances anti-tumor immunity. *Nat. Immunol.* 22:746–756. https://doi.org/10.1038/s41590-021-00940-2

Hanna, B.S., L. Llaó-Cid, M. Iskar, P.M. Roessner, L.C. Klett, J.K.L. Wong, Y. Paul, N. Ioannou, S. Öztürk, N. Mack, et al. 2021. Interleukin-10 receptor signaling promotes the maintenance of a PD-1^{int} TCF-1$^+$ CD8$^+$ T cell population that sustains anti-tumor immunity. *Immunity*. 54:2825–2841.e10. https://doi.org/10.1016/j.immuni.2021.11.004

Hermans, D., S. Gautam, J.C. García-Cañaveras, D. Gromer, S. Mitra, R. Spolski, P. Li, S. Christensen, R. Nguyen, J.X. Lin, et al. 2020. Lactate dehydrogenase inhibition synergizes with IL-21 to promote CD8$^+$ T cell stemness and antitumor immunity. *Proc. Natl. Acad. Sci. USA*. 117:6047–6055. https://doi.org/10.1073/pnas.1920413117

Hirahara, K., A. Onodera, A.V. Villarino, M. Bonelli, G. Sciumè, A. Laurence, H.W. Sun, S.R. Brooks, G. Vahedi, H.Y. Shih, et al. 2015. Asymmetric action of STAT transcription factors drives transcriptional outputs and cytokine specificity. *Immunity*. 42:877–889. https://doi.org/10.1016/j.immuni.2015.04.014

Huang, Q., X. Wu, Z. Wang, X. Chen, L. Wang, Y. Lu, D. Xiong, Q. Liu, Y. Tian, H. Lin, et al. 2022. The primordial differentiation of tumor-specific memory CD8$^+$ T cells as bona fide responders to PD-1/PD-L1 blockade in draining lymph nodes. *Cell*. 185:4049–4066.e25. https://doi.org/10.1016/j.cell.2022.09.020

Huang, Z., J. Zak, I. Pratumchai, N. Shaabani, V.F. Vartabedian, N. Nguyen, T. Wu, C. Xiao, and J.R. Teijaro. 2019. IL-27 promotes the expansion of self-renewing CD8$^+$ T cells in persistent viral infection. *J. Exp. Med.* 216:1791–1808. https://doi.org/10.1084/jem.20190173

Huynh, J., A. Chand, D. Gough, and M. Ernst. 2019. Therapeutically exploiting STAT3 activity in cancer - using tissue repair as a road map. *Nat. Rev. Cancer*. 19:82–96. https://doi.org/10.1038/s41568-018-0090-8

Jiang, Z., R. Liao, J. Lv, S. Li, D. Zheng, L. Qin, D. Wu, S. Chen, Y. Long, Q. Wu, et al. 2020. IL-6 trans-signaling promotes the expansion and anti-tumor activity of CAR T cells. *Leukemia*. 35:1380–1391. https://doi.org/10.1038/s41375-020-01085-1

Joshi, N.S., W. Cui, A. Chandele, H.K. Lee, D.R. Urso, J. Hagman, L. Gapin, and S.M. Kaech. 2007. Inflammation directs memory precursor and short-lived effector CD8(+) T cell fates via the graded expression of T-bet transcription factor. *Immunity*. 27:281–295. https://doi.org/10.1016/j.immuni.2007.07.010

Kaech, S.M., and W. Cui. 2012. Transcriptional control of effector and memory CD8$^+$ T cell differentiation. *Nat. Rev. Immunol.* 12:749–761. https://doi.org/10.1038/nri3307

Kagoya, Y., S. Tanaka, T. Guo, M. Anczurowski, C.H. Wang, K. Saso, M.O. Butler, M.D. Minden, and N. Hirano. 2018. A novel chimeric antigen receptor containing a JAK-STAT signaling domain mediates superior antitumor effects. *Nat. Med.* 24:352–359. https://doi.org/10.1038/nm.4478

Kamphorst, A.O., A. Wieland, T. Nasti, S. Yang, R. Zhang, D.L.Barber, B.T.Konieczny, C.Z.Daugherty, L.Koenig, K.Yu, et al. 2017. Rescue of exhausted CD8 T cells by PD-1–targeted therapies is CD28-dependent. *Science*. 355:1423–1427. https://doi.org/10.1126/science.aaf0683

Kane, A., E.K. Deenick, C.S. Ma, M.C. Cook, G. Uzel, and S.G. Tangye. 2014. STAT3 is a central regulator of lymphocyte differentiation and function. *Curr. Opin. Immunol.* 28:49–57. https://doi.org/10.1016/j.coi.2014.01.015

Khan, O., J.R. Giles, S. McDonald, S. Manne, S.F. Ngiow, K.P. Patel, M.T. Werner, A.C. Huang, K.A. Alexander, J.E. Wu, et al. 2019. TOX transcriptionally and epigenetically programs CD8$^+$ T cell exhaustion. *Nature*. 571:211–218. https://doi.org/10.1038/s41586-019-1325-x

Kurachi, M., R.A. Barnitz, N. Yosef, P.M. Odorizzi, M.A. DiIorio, M.E. Lemieux, K. Yates, J. Godec, M.G. Klatt, A. Regev, et al. 2014. The transcription factor BATF operates as an essential differentiation checkpoint in early effector CD8$^+$ T cells. *Nat. Immunol.* 15:373–383. https://doi.org/10.1038/ni.2834

Kwon, H., D. Thierry-Mieg, J. Thierry-Mieg, H.P. Kim, J. Oh, C. Tunyaplin, S. Carotta, C.E. Donovan, M.L. Goldman, P. Tailor, et al. 2009. Analysis of interleukin-21-induced Prdm1 gene regulation reveals functional cooperation of STAT3 and IRF4 transcription factors. *Immunity*. 31:941–952. https://doi.org/10.1016/j.immuni.2009.10.008

Langmead, B., and S.L. Salzberg. 2012. Fast gapped-read alignment with Bowtie 2. *Nat. Methods*. 9:357–359. https://doi.org/10.1038/nmeth.1923

Li, P., and W.J. Leonard. 2018. Chromatin accessibility and interactions in the transcriptional regulation of T cells. *Front. Immunol.* 9:2738. https://doi.org/10.3389/fimmu.2018.02738

Liu, X., Y. Wang, H. Lu, J. Li, X. Yan, M. Xiao, J. Hao, A. Alekseev, H. Khong, T. Chen, et al. 2019. Genome-wide analysis identifies NR4A1 as a key mediator of T cell dysfunction. *Nature*. 567:525–529. https://doi.org/10.1038/s41586-019-0979-8

Liu, Y., N. Zhou, L. Zhou, J. Wang, Y. Zhou, T. Zhang, Y. Fang, J. Deng, Y. Gao, X. Liang, et al. 2021. IL-2 regulates tumor-reactive CD8$^+$ T cell exhaustion by activating the aryl hydrocarbon receptor. *Nat. Immunol.* 22:358–369. https://doi.org/10.1038/s41590-020-00850-9

Ma, X., P. Shou, C. Smith, Y. Chen, H. Du, C. Sun, N. Porterfield Kren, D. Michaud, S. Ahn, B. Vincent, et al. 2020. Interleukin-23 engineering improves CAR T cell function in solid tumors. *Nat. Biotechnol.* 38:448–459. https://doi.org/10.1038/s41587-019-0398-2

Maekawa, Y., Y. Minato, C. Ishifune, T. Kurihara, A. Kitamura, H. Kojima, H. Yagita, M. Sakata-Yanagimoto, T. Saito, I. Taniuchi, et al. 2008. Notch2 integrates signaling by the transcription factors RBP-J and CREB1 to promote T cell cytotoxicity. *Nat. Immunol.* 9:1140–1147. https://doi.org/10.1038/ni.1649

Man, K., S.S. Gabriel, Y. Liao, R. Gloury, S. Preston, D.C. Henstridge, M. Pellegrini, D. Zehn, F. Berberich-Siebelt, M.A. Febbraio, et al. 2017. Transcription factor IRF4 promotes CD8$^+$ T cell exhaustion and limits the development of memory-like T cells during chronic infection. *Infect. Immun.* 47:1129–1141.e5. https://doi.org/10.1016/j.immuni.2017.11.021

Martinez, G.J., R.M. Pereira, T. Äijö, E.Y. Kim, F. Marangoni, M.E. Pipkin, S. Togher, V. Heissmeyer, Y.C. Zhang, S. Crotty, et al. 2015. The transcription factor NFAT promotes exhaustion of activated CD8$^+$ T cells. *Immunity*. 42:265–278. https://doi.org/10.1016/j.immuni.2015.01.006

McFarland-Mancini, M.M., H.M. Funk, A.M. Paluch, M. Zhou, P.V. Giridhar, C.A. Mercer, S.C. Kozma, and A.F. Drew. 2010. Differences in wound healing in mice with deficiency of IL-6 versus IL-6 receptor. *J. Immunol.* 184:7219–7228. https://doi.org/10.4049/jimmunol.0901929

McLane, L.M., M.S. Abdel-Hakeem, and E.J. Wherry. 2019. CD8 T cell exhaustion during chronic viral infection and cancer. *Annu. Rev. Immunol.* 37:457–495. https://doi.org/10.1146/annurev-immunol-041015-055318

Miller, B.C., D.R. Sen, R. Al Abosy, K. Bi, Y.V. Virkud, M.W. LaFleur, K.B. Yates, A. Lako, K. Felt, G.S. Naik, et al. 2019. Subsets of exhausted CD8$^+$ T cells differentially mediate tumor control and respond to checkpoint blockade. *Nat. Immunol.* 20:326–336. https://doi.org/10.1038/s41590-019-0312-6

Mujib, S., R.B. Jones, C. Lo, N. Aidarus, K. Clayton, A. Sakhdari, E. Benko, C. Kovacs, and M.A. Ostrowski. 2012. Antigen-independent induction of Tim-3 expression on human T cells by the common γ-chain cytokines IL-2, IL-7, IL-15, and IL-21 is associated with proliferation and is dependent on the phosphoinositide 3-kinase pathway. *J. Immunol.* 188: 3745–3756. https://doi.org/10.4049/jimmunol.1102609

Nurieva, R.I., Y. Chung, G.J. Martinez, X.O. Yang, S. Tanaka, T.D. Matskevitch, Y.H. Wang, and C. Dong. 2009. Bcl6 mediates the development of T follicular helper cells. *Science*. 325:1001–1005. https://doi.org/10.1126/science.1176676

Olson, J.A., and S.C. Jameson. 2011. Keeping STATs on memory CD8$^+$ T cells. *Immunity*. 35:663–665. https://doi.org/10.1016/j.immuni.2011.11.006

Owaki, T., M. Asakawa, N. Morishima, I. Mizoguchi, F. Fukai, K. Takeda, J. Mizuguchi, and T. Yoshimoto. 2008. STAT3 is indispensable to IL-27-mediated cell proliferation but not to IL-27-induced Th1 differentiation and suppression of proinflammatory cytokine production. *J. Immunol.* 180:2903–2911. https://doi.org/10.4049/jimmunol.180.5.2903

Pauken, K.E., and E.J. Wherry. 2015. SnapShot: T cell exhaustion. *Cell*. 163: 1038–1038.e1. https://doi.org/10.1016/j.cell.2015.10.054

Philip, M., and A. Schietinger. 2021. CD8(+) T cell differentiation and dysfunction in cancer. *Nat. Rev. Immunol.* 22:209–223. https://doi.org/10.1038/s41577-021-00574-3

Puram, S.V., I. Tirosh, A.S. Parikh, A.P. Patel, K. Yizhak, S. Gillespie, C. Rodman, C.L. Luo, E.A. Mroz, K.S. Emerick, et al. 2017. Single-cell transcriptomic analysis of primary and metastatic tumor ecosystems in head and neck cancer. *Cell*. 171:1611–1624 e24. https://doi.org/10.1016/j.cell.2017.10.044

Ramírez, F., D.P. Ryan, B. Grüning, V. Bhardwaj, F. Kilpert, A.S. Richter, S. Heyne, F. Dündar, and T. Manke. 2016. deepTools2: A next generation web server for deep-sequencing data analysis. *Nucleic Acids Res.* 44: W160–W165. https://doi.org/10.1093/nar/gkw257

Ren, H.M., E.M. Kolawole, and M. Ren. 2020. IL-21 from high-affinity CD4 T cells drives differentiation of brain-resident CD8 T cells during persistent viral infection. *Sci. Immunol.* 5:eabb5590. https://doi.org/10.1126/sciimmunol.abb5590

Rutishauser, R.L., G.A. Martins, S. Kalachikov, A. Chandele, I.A. Parish, E. Meffre, J. Jacob, K. Calame, and S.M. Kaech. 2009. Transcriptional repressor Blimp-1 promotes CD8(+) T cell terminal differentiation and represses the acquisition of central memory T cell properties. *Immunity*. 31:296–308. https://doi.org/10.1016/j.immuni.2009.05.014

Ryan, N., K. Anderson, G. Volpedo, O. Hamza, S. Varikuti, A.R. Satoskar, and S. Oghumu. 2020. STAT1 inhibits T-cell exhaustion and myeloid derived suppressor cell accumulation to promote antitumor immune responses in head and neck squamous cell carcinoma. *Int. J. Cancer*. 146: 1717–1729. https://doi.org/10.1002/ijc.32781

Sade-Feldman, M., K. Yizhak, S.L. Bjorgaard, J.P. Ray, C.G. de Boer, R.W. Jenkins, D.J. Lieb, J.H. Chen, D.T. Frederick, M. Barzily-Rokni, et al. 2018. Defining T cell states associated with response to checkpoint immunotherapy in melanoma. *Cell*. 175:998–1013.e20. https://doi.org/10.1016/j.cell.2018.10.038

Sawant, D.V., H. Yano, M. Chikina, Q. Zhang, M. Liao, C. Liu, D.J. Callahan, Z. Sun, T. Sun, T. Tabib, et al. 2019. Adaptive plasticity of IL-10$^+$ and IL-35$^+$ T_{reg} cells cooperatively promotes tumor T cell exhaustion. *Nat. Immunol.* 20:724–735. https://doi.org/10.1038/s41590-019-0346-9

Schenkel, J.M., R.H. Herbst, D. Canner, A. Li, M. Hillman, S.L. Shanahan, G. Gibbons, O.C. Smith, J.Y. Kim, P. Westcott, et al. 2021. Conventional type I dendric cells maintain a reservoir of proliferative tumor-antigen specific TCF-1(+) CD8(+) T cells in tumor-draining lymph nodes. *Immunity*. 54:2338–2353.e6. https://doi.org/10.1016/j.immuni.2021.08.026

Scott, A.C., F. Dündar, P. Zumbo, S.S. Chandran, C.A. Klebanoff, M. Shakiba, P. Trivedi, L. Menocal, H. Appleby, S. Camara, et al. 2019. TOX is a critical regulator of tumour-specific T cell differentiation. *Nature*. 571: 270–274. https://doi.org/10.1038/s41586-019-1324-y

Seo, H., E. González-Avalos, W. Zhang, P. Ramchandani, C. Yang, C.J. Lio, A. Rao, and P.G. Hogan. 2021. BATF and IRF4 cooperate to counter exhaustion in tumor-infiltrating CAR T cells. *Nat. Immunol.* 22:983–995. https://doi.org/10.1038/s41590-021-00964-8

Siddiqui, I., K. Schaeuble, V. Chennupati, S.A. Fuertes Marraco, S. Calderon-Copete, D. Pais Ferreira, S.J. Carmona, L. Scarpellino, D. Gfeller, S. Pradervand, et al. 2019. Intratumoral Tcf1$^+$PD-1$^+$CD8$^+$ T cells with stem-like properties promote tumor control in response to vaccination and checkpoint blockade Immunotherapy. *Immunity*. 50:195–211.e10. https://doi.org/10.1016/j.immuni.2018.12.021

Siegel, A.M., J. Heimall, A.F. Freeman, A.P. Hsu, E. Brittain, J.M. Brenchley, D.C. Douek, G.H. Fahle, J.I. Cohen, S.M. Holland, and J.D. Milner. 2011. A critical role for STAT3 transcription factor signaling in the development and maintenance of human T cell memory. *Immunity*. 35:806–818. https://doi.org/10.1016/j.immuni.2011.09.016

Snell, L.M., B.L. MacLeod, J.C. Law, I. Osokine, H.J. Elsaesser, K. Hezaveh, R.J. Dickson, M.A. Gavin, C.J. Guidos, T.L. McGaha, and D.G. Brooks. 2018. CD8$^+$ T cell priming in established chronic viral infection preferentially directs differentiation of memory-like cells for sustained immunity. *Immunity*. 49:678–694.e5. https://doi.org/10.1016/j.immuni.2018.08.002

Takeda, K., T. Kaisho, N. Yoshida, J. Takeda, T. Kishimoto, and S. Akira. 1998. Stat3 activation is responsible for IL-6-dependent T cell proliferation through preventing apoptosis: Generation and characterization of T cell-specific stat3-deficient mice. *J. Immunol.* 161:4652–4660

Vahedi, G., H. Takahashi, S. Nakayamada, H.W. Sun, V. Sartorelli, Y. Kanno, and J.J. O'Shea. 2012. STATs shape the active enhancer landscape of T cell populations. *Cell*. 151:981–993. https://doi.org/10.1016/j.cell.2012.09.044

Wegrzyn, J., R. Potla, Y.-J. Chwae, N.B. Sepuri, Q. Zhang, T. Koeck, M. Derecka, K. Szczepanek, M. Szelag, A. Gornicka, et al. 2009. Function of mitochondrial Stat3 in cellular respiration. *Science*. 323:793–797. https://doi.org/10.1126/science.1164551

Wen, Z., Z. Zhong, and J.E. Darnell Jr. 1995. Maximal activation of transcription by statl and stat3 requires both tyrosine and serine phosphorylation. *Cell*. 82:241–250. https://doi.org/10.1016/0092-8674(95)90311-9

Wu, T., Y. Ji, E.A. Moseman, H.C. Xu, M. Manglani, M. Kirby, S.M. Anderson, R. Handon, E. Kenyon, A. Elkahloun, et al. 2016. The TCF1-Bcl6 axis counteracts type I interferon to repress exhaustion and maintain T cell stemness. *Sci. Immunol.* 1:eaai8593. https://doi.org/10.1126/sciimmunol.aai8593

Xin, G., D.M. Schauder, B. Lainez, J.S. Weinstein, Z. Dai, Y. Chen, E. Esplugues, R. Wen, D. Wang, I.A. Parish, et al. 2015. A critical role of IL-21-induced BATF in sustaining CD8-T-cell-mediated chronic viral control. *Cell Rep.* 13:1118–1124. https://doi.org/10.1016/j.celrep.2015.09.069

Xu, W., X. Zhao, X. Wang, H. Feng, M. Gou, W. Jin, X. Wang, X. Liu, and C. Dong. 2019. The transcription factor Tox2 drives T follicular helper cell development via regulating chromatin accessibility. *Immunity*. 51: 826–839.e5. https://doi.org/10.1016/j.immuni.2019.10.006

Yang, R., A.R. Masters, K.A. Fortner, D.P. Champagne, N. Yanguas-Casás, D.J. Silberger, C.T. Weaver, L. Haynes, and M. Rincon. 2016. IL-6 promotes the differentiation of a subset of naive CD8$^+$ T cells into IL-21-producing B helper CD8$^+$ T cells. *J. Exp. Med.* 213:2281–2291. https://doi.org/10.1084/jem.20160417

Yang, X.O., A.D. Panopoulos, R. Nurieva, S.H. Chang, D. Wang, S.S. Watowich, and C. Dong. 2007. STAT3 regulates cytokine-mediated generation of inflammatory helper T cells. *J. Biol. Chem.* 282:9358–9363. https://doi.org/10.1074/jbc.C600321200

Yang, Z.Z., D.M. Grote, S.C. Ziesmer, T. Niki, M. Hirashima, A.J. Novak, T.E. Witzig, and S.M. Ansell. 2012. IL-12 upregulates TIM-3 expression and induces T cell exhaustion in patients with follicular B cell non-Hodgkin

lymphoma. *J. Clin. Invest.* 122:1271–1282. https://doi.org/10.1172/JCI59806

Yi, J.S., M. Du, and A.J. Zajac. 2009. A vital role for interleukin-21 in the control of a chronic viral infection. *Science*. 324:1572–1576. https://doi.org/10.1126/science.1175194

You, L., Z. Wang, H. Li, J. Shou, Z. Jing, J. Xie, X. Sui, H. Pan, and W. Han. 2015. The role of STAT3 in autophagy. *Autophagy*. 11:729–739. https://doi.org/10.1080/15548627.2015.1017192

Yu, C.R., I.M. Dambuza, Y.J. Lee, G.M. Frank, and C.E. Egwuagu. 2013. STAT3 regulates proliferation and survival of CD8$^+$ T cells: Enhances effector responses to HSV-1 infection, and inhibits IL-10+ regulatory CD8$^+$ T cells in autoimmune uveitis. *Mediators Inflamm.* 2013:359674. https://doi.org/10.1155/2013/359674

Yu, G., L.G. Wang, and Q.Y. He. 2015. ChIPseeker: An R/Bioconductor package for ChIP peak annotation, comparison and visualization. *Bioinformatics*. 31:2382–2383. https://doi.org/10.1093/bioinformatics/btv145

Yu, H., H. Lee, A. Herrmann, R. Buettner, and R. Jove. 2014. Revisiting STAT3 signalling in cancer: New and unexpected biological functions. *Nat. Rev. Cancer*. 14:736–746. https://doi.org/10.1038/nrc3818

Yu, H., D. Pardoll, and R. Jove. 2009. STATs in cancer inflammation and immunity: A leading role for STAT3. *Nat. Rev. Cancer*. 9:798–809. https://doi.org/10.1038/nrc2734

Zander, R., M.Y. Kasmani, Y. Chen, P. Topchyan, J. Shen, S. Zheng, R. Burns, J. Ingram, C. Cui, N. Joshi, et al. 2022. Tfh-cell-derived interleukin 21 sustains effector CD8$^+$ T cell responses during chronic viral infection. *Immunity*. 55:475–493.e5. https://doi.org/10.1016/j.immuni.2022.01.018

Zander, R., D. Schauder, G. Xin, C. Nguyen, X. Wu, A. Zajac, and W. Cui. 2019. CD4$^+$ T cell Help is required for the formation of a cytolytic CD8$^+$ T cell subset that protects against chronic infection and cancer. *Immunity*. 51:1028–1042.e4. https://doi.org/10.1016/j.immuni.2019.10.009

Zhang, C., C. Yue, A. Herrmann, J. Song, C. Egelston, T. Wang, Z. Zhang, W. Li, H. Lee, M. Aftabizadeh, et al. 2020. STAT3 activation-induced fatty acid oxidation in CD8$^+$ T effector cells is critical for obesity-promoted breast tumor growth. *Cell Metabol.* 31:148–161.e5. https://doi.org/10.1016/j.cmet.2019.10.013

Zhang, L., X. Yu, L. Zheng, Y. Zhang, Y. Li, Q. Fang, R. Gao, B. Kang, Q. Zhang, J.Y. Huang, et al. 2018. Lineage tracking reveals dynamic relationships of T cells in colorectal cancer. *Nature*. 564:268–272. https://doi.org/10.1038/s41586-018-0694-x

Zhang, Y., T. Liu, C.A. Meyer, J. Eeckhoute, D.S. Johnson, B.E. Bernstein, C. Nusbaum, R.M. Myers, M. Brown, W. Li, and X.S. Liu. 2008. Model-based analysis of ChIP-seq (MACS). *Genome Biol.* 9:R137. https://doi.org/10.1186/gb-2008-9-9-r137

Zheng, C., L. Zheng, J.K. Yoo, H. Guo, Y. Zhang, X. Guo, B. Kang, R. Hu, J.Y. Huang, Q. Zhang, et al. 2017. Landscape of infiltrating T cells in liver cancer revealed by single-cell sequencing. *Cell*. 169:1342–1356.e16. https://doi.org/10.1016/j.cell.2017.05.035

Supplemental material

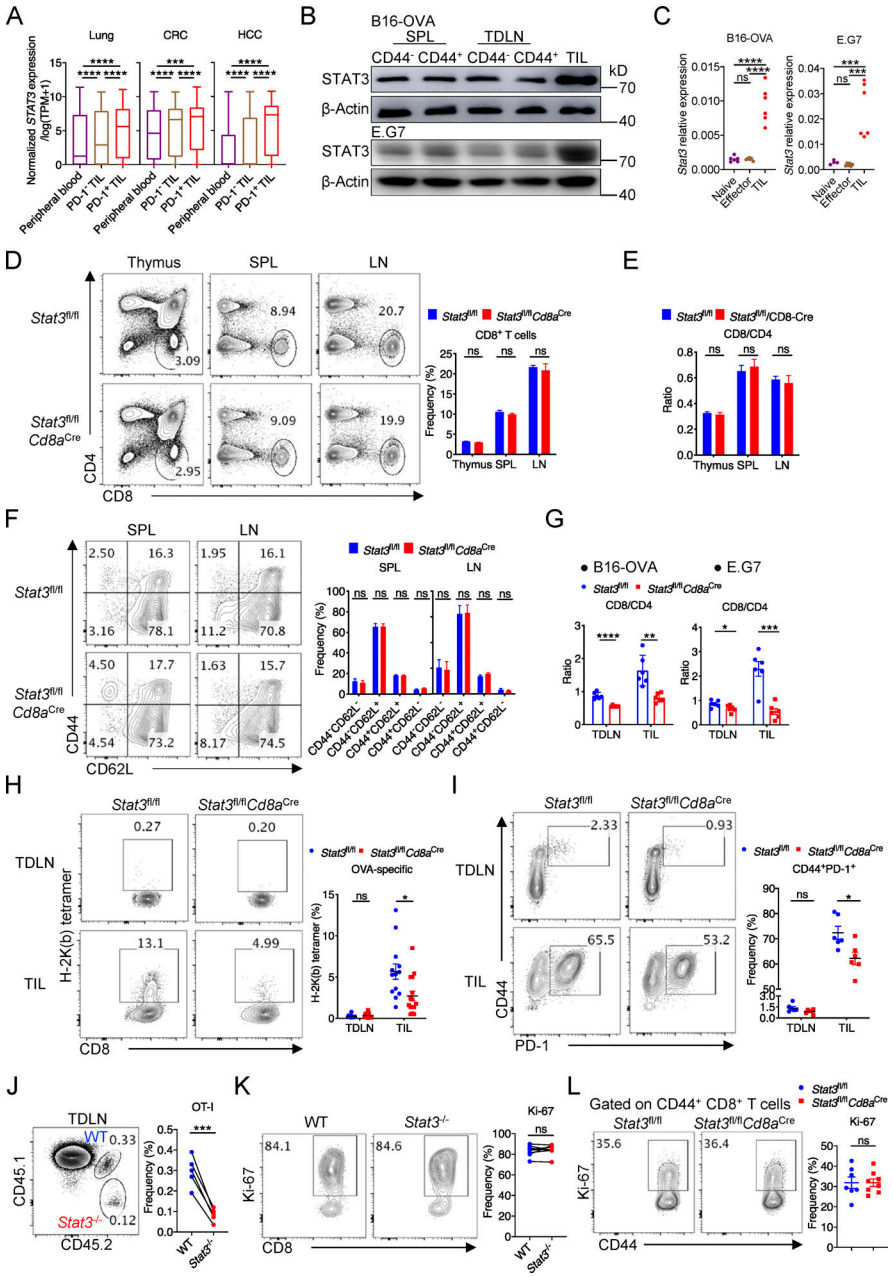

Figure S1. **STAT3 is intrinsically critical for the effector function of CD8⁺ T cells. (A)** mRNA level of *STAT3* in CD8⁺ T cells from peripheral blood or tumors in human cancer patients (GEO accession nos. GSE99254, GSE108989, and GSE98638). scRNA-seq data of CD8⁺ T cells in tumors and peripheral blood from lung, CRC, and HCC patients were previously processed and uploaded by others (http://crc.cancer-pku.cn/, http://hcc.cancer-pku.cn/, http://lung.cancer-pku.cn/; Guo et al., 2018; Zhang et al., 2018; Zheng et al., 2017), and we obtained the *STAT3* expression values from the above websites. The expression unit was normalized expression/$\log_2^{(TPM+1)}$. We compared the *STAT3* expression values in CD8⁺ T cells from peripheral blood, and in PD-1–negative (*PDCD1* expression value = 0) and –positive (*PDCD1* expression value >0) CD8⁺ T cells from tumors. **(B)** STAT3 protein expression in CD8⁺ T cells from spleens, TDLNs, and tumors in B16-OVA (upper plot) and E.G7 (bottom plot) models. **(C)** mRNA levels of *Stat3* in CD8⁺ T cells from TDLNs and tumors in B16-OVA (left panel) and E.G7 (right panel) models. **(D)** Frequencies of CD8⁺ T cells in thymuses, spleens, and lymph nodes in 6- to 8-wk-old $Stat3^{fl/fl}$ (n = 5) and $Stat3^{fl/fl}Cd8a^{Cre}$ (n = 5) mice. **(E)** Ratios of CD8⁺ T cells to CD4⁺ T cells in the thymuses, spleens, and lymph nodes from 6- to 8-wk-old $Stat3^{fl/fl}$ (n = 5) and $Stat3^{fl/fl}Cd8a^{Cre}$ (n = 5) mice. **(F)** Representative plots (left panel) and quantifications (right panel) of CD44 and CD62L expression on CD8⁺ T cells in the spleens and lymph nodes from 6- to 8-wk-old $Stat3^{fl/fl}$ (n = 5) and $Stat3^{fl/fl}Cd8a^{Cre}$ (n = 5) mice. **(G)** Ratios of CD8⁺ T cells to CD4⁺ T cells in TDLNs and tumors. **(H)** Representative plots (left panel) and quantifications (right panel) of H-2K(b) tetramer⁺ CD8⁺ T cells among total CD8⁺ T cells from TDLNs and E.G7 tumors. **(I)** Representative plots (left panel) and quantifications (right panel) of CD44⁺ PD-1⁺ CD8⁺ T cells among total CD8⁺ T cells from TDLNs and E.G7 tumors. **(J)** OT-I TIL frequencies among total CD8+T cells from TDLNs in B16-OVA model on day 20 after tumor inoculation. **(K)** Representative plots (left panel) and quantifications (right panel) of Ki-67 expression in OT-I TILs from B16-OVA tumors on day 20 after tumor inoculation. **(L)** Representative plots (left panel) and quantifications (right panel) of Ki-67 expression in splenic CD44⁺ CD8⁺ T cells on day 8 after LM-OVA infection. Data are pooled from three independent experiments (H), or are representative of two (B–F, G [left], J, and L) or three (G [right], I, and K) independent experiments. Data are shown as mean ± SEM. *, P < 0.05; **, P < 0.01; ***, P < 0.001; ****, P < 0.0001 by one-way ANOVA (A and C), unpaired two-tailed Student's t test (D–I and L) or paired two-tailed Student's t test (J and K). Source data are available for this figure: SourceData FS1.

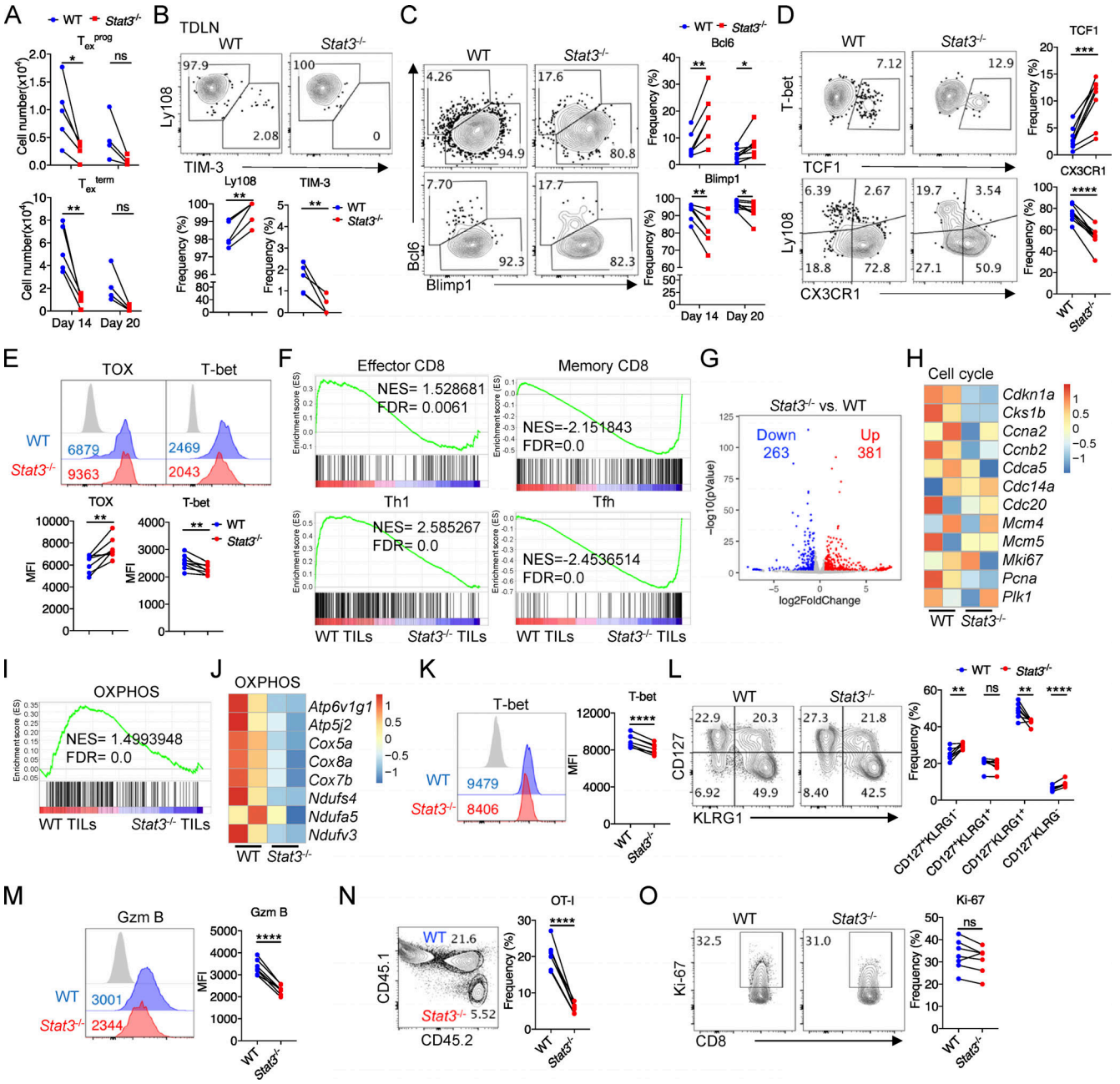

Figure S2. **STAT3 promotes the development of terminally differentiated CD8⁺ T cells. (A)** Numbers of T_{ex}^{prog} (upper panel) and T_{ex}^{term} (bottom panel) OT-I cells from B16-OVA tumors on day 14 and day 20 after tumor inoculation. **(B)** Representative plots (upper panel) and quantifications (bottom panel) of Ly108 and TIM-3 expression on OT-I cells from TDLNs in B16-OVA tumor model on day 20 after tumor inoculation. **(C)** Representative plots (left panel) and quantifications (right panel) of Bcl6 and Blimp1 expression in OT-I cells from B16-OVA tumors on day 14 and day 20 after tumor inoculation. **(D)** Representative plots (left panel) and quantifications (right panel) of TCF1 and CX3CR1 expression in/on OT-I cells from B16-OVA tumors on day 20 after tumor inoculation. **(E)** Representative plots (upper panel) and quantifications (bottom panel) of TOX and T-bet expression in OT-I cells from B16-OVA tumors on day 20 after tumor inoculation. **(F)** GSEA results for identifying gene signatures of WT and *Stat3*$^{-/-}$ OT-I TILs compared with other T cell subsets (GEO accession nos. GSE65660 and GSE8678). NES, normalized enrichment score; FDR, false discovery rate q-value. **(G)** Volcanic plot showing DEGs in WT and *Stat3*$^{-/-}$ OT-I TILs. **(H)** Heatmap illustrating the relative expression of signature genes related to cell cycle pathway in WT and *Stat3*$^{-/-}$ OT-I TILs. **(I)** GSEA result for identifying gene signatures of WT and *Stat3*$^{-/-}$ OT-I TILs compared to OXPHOS feature genes (GSEA: MM3893). NES, normalized enrichment score; FDR, false discovery rate q-value. **(J)** Heatmap illustrating the relative expression of signature genes related to OXPHOS pathway in WT and *Stat3*$^{-/-}$ OT-I TILs. **(K)** Representative plots (left panel) and quantification (right panel) of T-bet expression in splenic OT-I cells on day 8 after LM-OVA infection. **(L)** Representative plots (left panel) and quantifications (right panel) of CD127 and KLRG1 expression on splenic OT-I cells on day 8 after LM-OVA infection. **(M)** Representative plots (left panel) and quantification (right panel) of Granzyme B expression in TCF1⁻Granzyme B⁺ splenic OT-I cells on day 8 after LM-OVA infection. **(N)** OT-I cell frequencies among total splenic CD8+T cells on day 8 after LM-OVA infection. **(O)** Representative plots (left panel) and quantification (right panel) of Ki-67 expression in splenic OT-I cells on day 8 after LM-OVA infection. Data are representative of two (K–O) or three (A–E) independent experiments. Data are shown as mean ± SEM. *, P < 0.05; **, P < 0.01; ***, P < 0.001; ****, P < 0.0001 by paired two-tailed Student's *t* test (A–E and K–O).

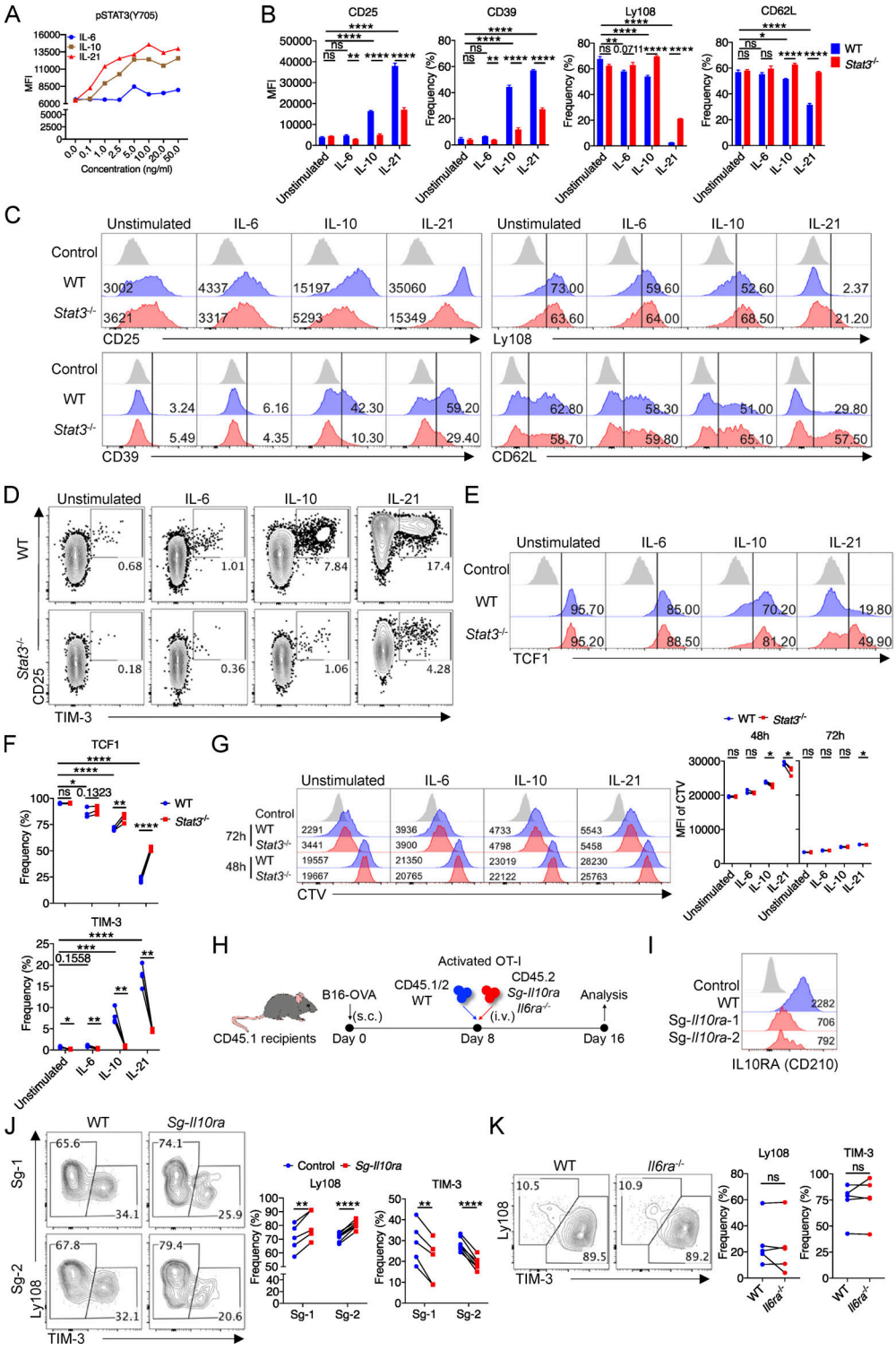

Figure S3. **IL-10 and IL-21 signaling intrinsically promotes the development of T_{ex}^{term} cells. (A)** Phosphorylation levels of STAT3 at the Y705 site in in vitro activated CD8⁺ T cells with the stimulation of IL-6, IL-10, or IL-21 for 30 min. **(B and C)** Quantifications (B) and representative plots (C) and of CD25, CD39, Ly108, and CD62L expression on in vitro–stimulated WT and *Stat3*$^{-/-}$ CD8⁺ T cells. **(D–F)** Representative plots (D and E) and quantifications (F) of TIM-3 and TCF1 expression on/in in vitro cocultured WT and *Stat3*$^{-/-}$ CD8⁺ T cells with the stimulation of IL-6, IL-10, or IL-21 for 3 d. **(G)** Proliferation of in vitro cocultured WT and *Stat3*$^{-/-}$ CD8⁺ T cells marked by CTV dilution. **(H)** Experimental design for adoptive cotransfer of WT and Sg-*Il10ra* or *Il6ra*$^{-/-}$ OT-I cells and B16-OVA tumor–challenge assay. **(I)** Representative plots of IL10RA (CD210) expression on WT and Sg-*Il10ra* OT-I TILs from B16-OVA tumors. **(J)** Representative plots (left panel) and quantifications (right panel) of Ly108 and TIM-3 expression on WT and Sg-*Il10ra* OT-I TILs from B16-OVA tumors. **(K)** Representative plots (left panel) and quantifications (right panel) of Ly108 and TIM-3 expression on WT and *Il6ra*$^{-/-}$ OT-I TILs from B16-OVA tumors. Data are representative of three (B–F, I, and K) or two (A, G, and J) independent experiments. Data are shown as mean ± SEM. *, P < 0.05; **, P < 0.01; ***, P < 0.001; ****, P < 0.0001 by unpaired two-tailed Student's *t* test (B) and paired two-tailed Student's *t* test (F, G, J, and K).

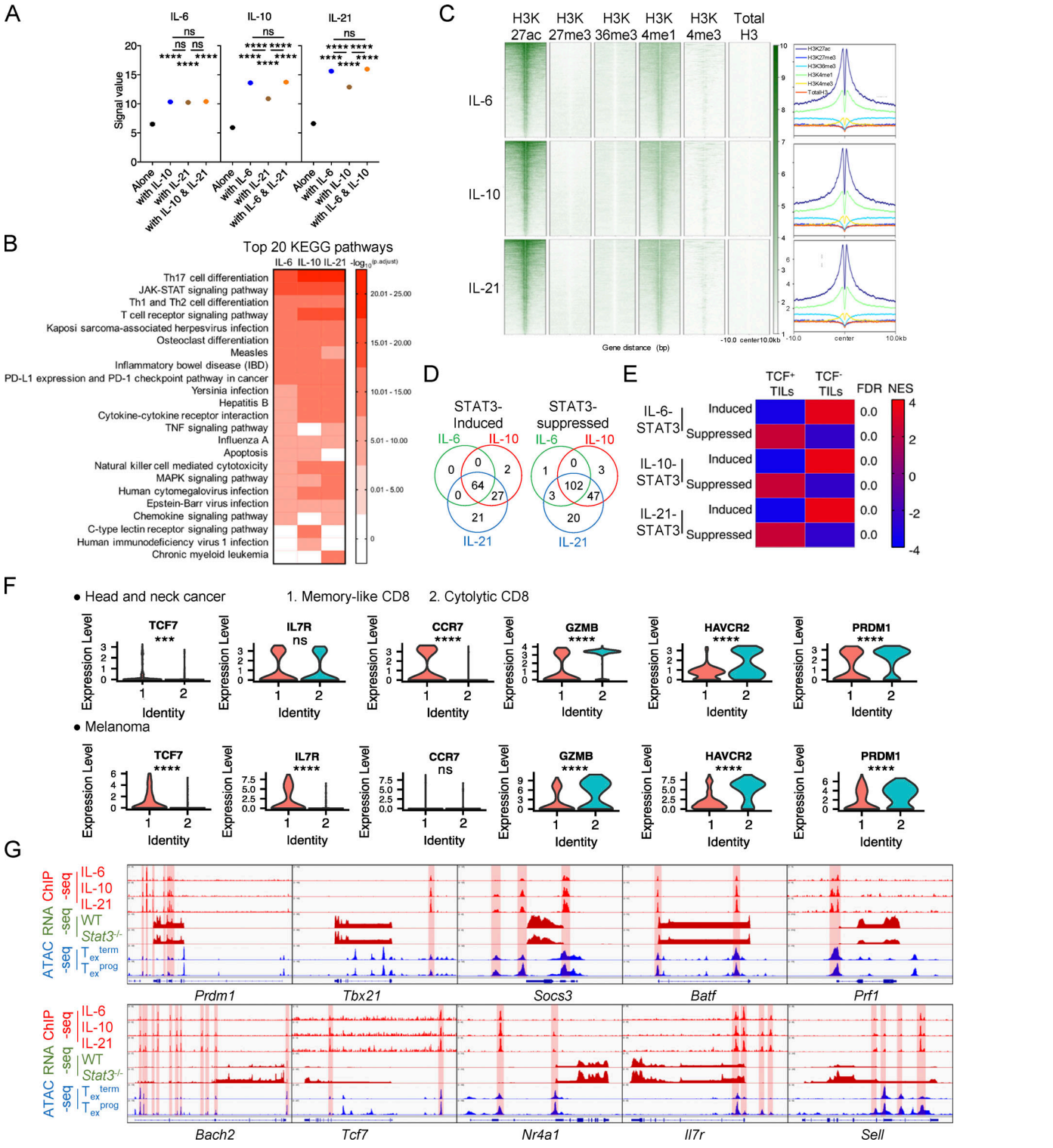

Figure S4. **STAT3 transcriptionally regulates T_{ex} cell differentiation. (A)** Signal values of pSTAT3-binding peaks in IL-6–, IL-10–, and IL-21–stimulated CD8⁺ T cells. **(B)** Top 20 KEGG pathways for pSTAT3-binding genes in in vitro activated CD8⁺ T cells with the stimulation of IL-6, IL-10, or IL-21. **(C)** Heatmaps and peak plots for read density profiles of H3K27ac, H3K27me3, H3K36me3, H3K4me1, and H3K4me3 occupations centered on pSTAT3-binding peaks (GEO accession no. GSE54191). Values were normalized to the total number of reads. **(D)** Venn diagrams of STAT3-regulated genes in in vitro activated CD8⁺ T cells with the stimulation of IL-6, IL-10, or IL-21. **(E)** GSEA results for comparing the enrichment of IL-6/10/21-STAT3 regulated genes in the transcriptomes of TCF1⁻ T_{ex}^{term} and TCF1⁺ T_{ex}^{prog} cells (GEO accession no. GSE114631). NES, normalized enrichment score; FDR, false discovery rate q-value. FDR presented as $-\log_{10}(FDR)$. **(F)** Violin plots illustrating the mRNA amounts of signature genes between tumor-infiltrating memory-like and cytolytic CD8⁺ T cells. (accession nos. GSE103322 and GSE120575). **(G)** pSTAT3 ChIP-seq tracks aligned with RNA-seq tracks of WT and *Stat3*$^{-/-}$ CD8⁺ TILs, and ATAC-seq tracks of T_{ex}^{prog} or T_{ex}^{term} cells at the specific gene loci (GEO accession no. GSE123236). Data are shown as mean ± SEM. *, P < 0.05; **, P < 0.01; ***, P < 0.001; ****, P < 0.0001 by unpaired two-tailed Student's *t* test (A and F).

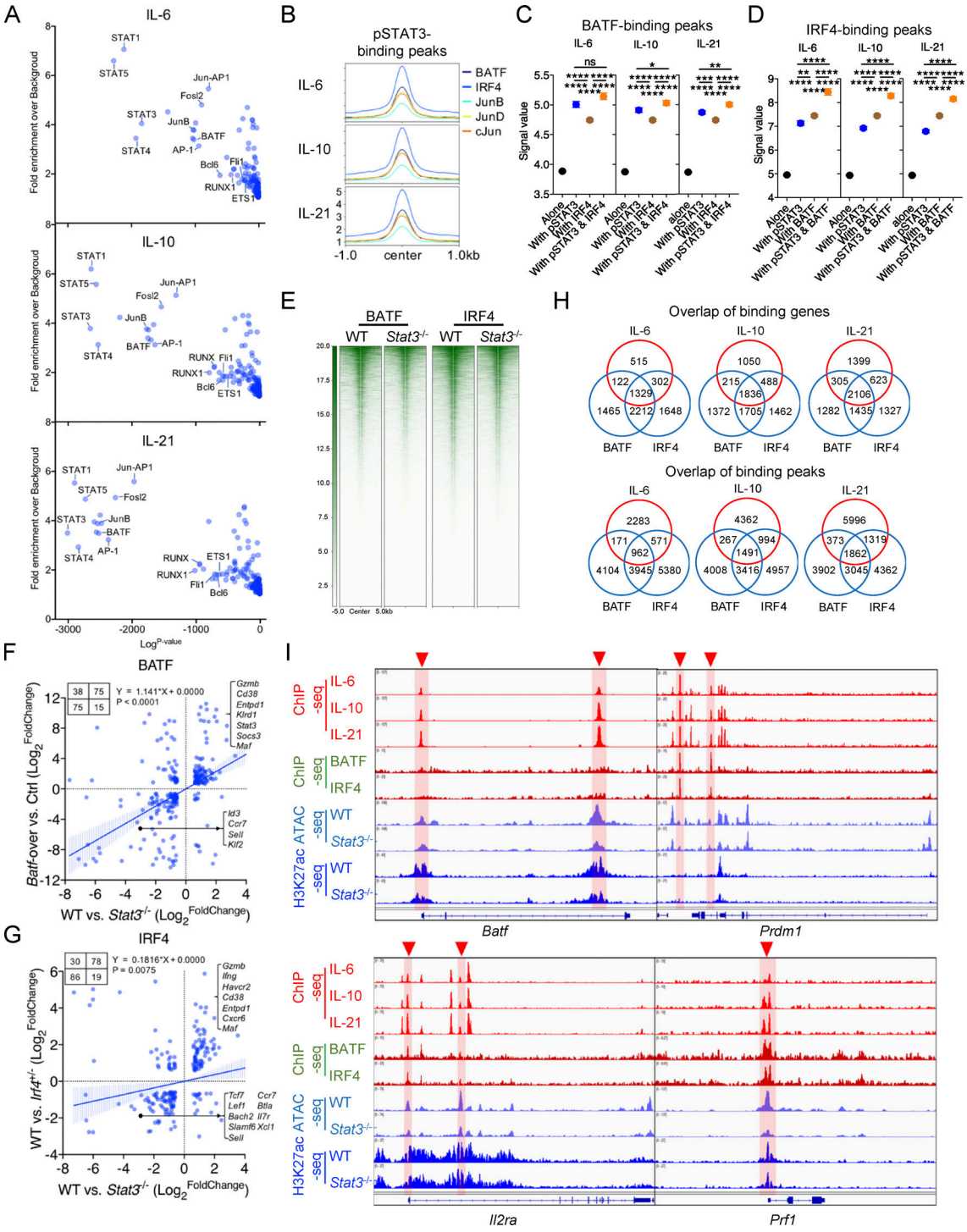

Figure S5. **STAT3 cooperates with BATF and IRF4 to mediate T_{ex}^{term} cell development. (A)** Enrichment of known transcription factor–binding motifs in pSTAT3-binding peaks. The x and y axes represent the $\log^{P\ value}$ and fold change of the motif enrichment separately. Targeted motifs were compared to the whole genome background to calculate P value and fold change. **(B)** Peak plots showing the read density profiles of BATF, IRF4, JunB, JunD, and c-Jun occupations centered on pSTAT3-binding peaks in CD8⁺ T cells (GEO accession no. GSE54191). Values were normalized to the total number of reads. **(C)** Signal values of BATF-binding peaks in CD8⁺ T cells at pSTAT3- or IRF4-binding sites or not (GEO accession no. GSE54191). **(D)** Signal values of IRF4-binding peaks in CD8⁺ T cells at pSTAT3- or BATF-binding sites or not (GEO accession no. GSE54191). **(E)** Heatmaps showing the deposition of H3K27ac modification centered on BATF- or IRF4-binding peaks in WT and *Stat3*$^{-/-}$ OT-I TILs (accession GEO: GSE54191). **(F)** Correlation analysis for DEGs identified in BATF- and STAT3-relevant RNA-seq (GEO accession no. GSE154745). DEGs were filtered by fold change >1.5 and P value <0.05. **(G)** Correlation analysis for DEGs identified in IRF4- and STAT3-relevant RNA-seq (GEO accession no. GSE84820). DEGs were filtered by fold change >1.5 and P value <0.05. **(H)** Venn diagram of pSTAT3-, BATF-, and IRF4-binding peaks and genes. **(I)** Aligned ChIP-seq tracks of pSTAT3, BATF, and IRF4 in CD8⁺ T cells, ATAC-seq tracks of WT and *Stat3*$^{-/-}$ OT-I TILs, and H3K27ac ChIP-seq tracks of WT and *Stat3*$^{-/-}$ CD8⁺ T cells at the specific gene loci. Data are shown as mean ± SEM. *, P < 0.05; **, P < 0.01; ***, P < 0.001; ****, P < 0.0001 by unpaired two-tailed Student's *t* test (C and D).

Provided online are Table S1, Table S2, Table S3, Table S4, Table S5, and Table S6. Table S1 lists DEGs in WT vs. *Stat3*$^{-/-}$ OT-I cells from B16-OVA tumors. Table S2 lists STAT3-binding and -regulated genes. Table S3 lists STAT3-induced or -suppressed feature genes. Table S4 lists DA peaks in WT vs. *Stat3*$^{-/-}$ OT-I cells from B16-OVA tumors. Table S5 lists differentially H3K27ac modified regions (DMRs) between IL-10–stimulated WT and *Stat3*$^{-/-}$ CD8^{+} T cells. Table S6 lists STAT3- and BATF/IRF4-coregulated genes.